Paradoxical dominant negative activity of an immunodeficiency-associated activating *PIK3R1* variant

Patsy R. Tomlinson[1,2,3], Rachel Knox[1,2,3], Olga Perisic[4], Helen C. Su[6], Gemma V. Brierley[1,2,3], Roger L. Williams[4], Robert K. Semple[3,5,7]

[1] The University of Cambridge Metabolic Research Laboratories, Wellcome Trust-MRC Institute of Metabolic Science, Cambridge, UK
[2] The National Institute for Health Research Cambridge Biomedical Research Centre, Cambridge, UK
[3] MRC Metabolic Diseases Unit, Wellcome Trust-MRC Institute of Metabolic Science, Cambridge, UK
[4] MRC Laboratory of Molecular Biology, Cambridge, UK
[5] Centre for Cardiovascular Science, University of Edinburgh, Edinburgh, UK
[6] Laboratory of Clinical Immunology & Microbiology, Intramural Research Program, National Institute of Allergy and Infectious Disease, National Institutes of Health, Bethesda, MD, USA
[7] MRC Human Genetics Unit, Institute of Genetics and Cancer, University of Edinburgh, Edinburgh, UK

Correspondence to:

Prof. Robert K. Semple, Centre for Cardiovascular Science, University of Edinburgh, Queen's Medical Research Institute, Little France Crescent, Edinburgh EH16 4TJ, UK. Tel: +44 131 242 6051/ Email: rsemple@ed.ac.uk

Character Count: 50,222 (to end of references; with spaces)

Running Title: Dominant negative effect of an activating PIK3R1 variant

Abstract

PIK3R1 encodes three regulatory subunits of class IA phosphoinositide 3-kinase (PI3K), each associating with any of three catalytic subunits, namely p110α, p110β or p110δ. Constitutional *PIK3R1* mutations cause diseases with a genotype-phenotype relationship not yet fully explained: heterozygous loss-of-function mutations cause SHORT syndrome, featuring insulin resistance and short stature attributed to reduced p110α function, while heterozygous activating mutations cause immunodeficiency, attributed to p110δ activation and known as APDS2. Surprisingly, APDS2 patients do not show features of p110α hyperactivation, but do commonly have short stature or SHORT syndrome, suggesting p110α hypofunction. We sought to investigate this. In dermal fibroblasts from an APDS2 patient, we found no increased PI3K signalling, with p110δ expression markedly reduced. In preadipocytes, the APDS2 variant was potently dominant negative, associating with Irs1 and Irs2 but failing to heterodimerise with p110α. This attenuation of p110α signalling by a p110δ-activating PIK3R1 variant potentially explains co-incidence of gain-of-function and loss-of-function *PIK3R1* phenotypes.

Keywords: APDS2, cancer, immunodeficiency, insulin resistance, phosphoinositide 3-kinase, PIK3R1, SHORT syndrome

Introduction

PIK3R1 gene products (p85α, p55α and p50α) are essential for class IA phosphoinositide 3-kinase (PI3K) signalling. Each of the three protein products can bind any of three catalytic subunits, p110α, β and δ, encoded by *PIK3CA*, *PIK3CB*, and *PIK3CD* respectively. This stabilises and inhibits the catalytic subunits in the basal state and confers responsiveness to upstream stimuli including receptor tyrosine kinase activation, enabled by two phosphotyrosine-binding SH2 domains shared by all PIK3R1 products (Fruman *et al*, 2017).

PI3K signalling mediates responses to a myriad of cues, including growth factors, hormones such as insulin, and processed antigens, and so recent discovery that genetic perturbation of PIK3R1 in humans disrupts growth, insulin action and immunity is no surprise. Beyond this headline observation lies considerable complexity, however, and important questions about genotype-phenotype correlations in PIK3R1-related disorders are unresolved.

Some PIK3R1 mutations reduce basal inhibition of catalytic subunits, usually due to disruption of the inhibitory inter-SH2 domain, and are found in cancers (Philp *et al*, 2001) and vascular malformations with overgrowth(Cottrell *et al*, 2021). In both diseases, hyperactivated PI3Kα, composed of heterodimers of *PIK3R1* products and p110α, drives pathological growth. Distinct inter-SH2 domain *PIK3R1* mutations, mostly causing skipping of exon 11 and deletion of residues 434-475, hyperactivate PI3Kδ in immune cells, causing immunodeficiency (Deau *et al*, 2014; Lucas *et al*, 2014b). This phenocopies the immunodeficiency caused by genetic activation of p110δ itself, called Activated PI3K Delta Syndrome 1 (APDS1) (Angulo *et al*, 2013; Lucas *et al*, 2014a), and is thus named APDS2.

Despite ubiquitous *PIK3R1* expression, features attributable to PI3Kα activation have been described in only a single case of APDS2 to date (Wentink *et al*, 2017). In that case, the causal variant was a constitutional activating mutation associated with cancer rather than one of the common APDS2 variants. Biochemical studies have suggested that apparently selective p110δ activation occurs because APDS2 mutations derepress p110δ, the

predominant immune system catalytic subunit, more than p110α, due to differences in the inhibitory contacts between *PIK3R1* products and different catalytic subunits (Dornan *et al*, 2017).

More surprisingly, phenotypic overlap is reported between APDS2 and SHORT syndrome. SHORT syndrome is caused by loss of PI3Kα function due to disruption of the phosphotyrosine-binding C-terminal SH2 domain (Chudasama *et al*, 2013; Dyment *et al*, 2013; Thauvin-Robinet *et al*, 2013). It features reduced linear growth, insulin resistance, and dysmorphic features (Avila *et al*, 2016). In recent years, both case reports (Bravo Garcia-Morato *et al*, 2017; Petrovski *et al*, 2016; Ramirez *et al*, 2020; Szczawinska-Poplonyk *et al*, 2022) and larger series (Elkaim *et al*, 2016; Jamee *et al*, 2020; Maccari *et al*, 2023; Nguyen *et al*, 2023; Olbrich *et al*, 2016; Petrovski *et al.*, 2016) have established that many people with APDS2 have overt features of SHORT syndrome, while, more generally, linear growth impairment is common in APDS2, but not in APDS1. These clinical observations are bolstered by the impaired linear growth and increased *in utero* mortality reported in mice with knock in of the common causal APDS2 mutation in Pik3r1(Nguyen *et al.*, 2023). All people with SHORT-APDS2 overlap syndromes have well established activating PIK3R1 mutations in the inter-SH2 domain implicated in APDS2, but none have characteristic SHORT syndrome mutations, which are usually in the C-terminal SH2 domain. Conversely, no patient with a classical SHORT syndrome mutation has been shown to have immunodeficiency. There is thus now convincing evidence of a syndrome with features of both gain and loss of PI3K function. The mechanistic basis of this is unexplained.

PI3K activity is determined not just by activity of individual PI3K holoenzymes, but also by subunit stoichiometry. Regulatory and catalytic subunits stabilise each other upon binding (Brachmann *et al*, 2005; Yu *et al*, 1998), and only regulatory subunit monomers are stable enough to be detected in mammalian cells (Yu *et al.*, 1998). Molar excess of regulatory subunits over catalytic subunits gives rise to free regulatory subunits that compete with holoenzyme for phosphotyrosine binding (Ueki *et al*, 2002). This has been invoked to explain

increased insulin sensitivity on knockout or reduction of p85α alone (Mauvais-Jarvis *et al*, 2002), of p55α and p50α (Chen *et al*, 2004) or of all *Pik3r1* products (Fruman *et al*, 2000). The "free-p85" model has been contested by some reports suggesting no excess p85 (Geering *et al*, 2007; Zhao *et al*, 2006), however most observations, including some made recently using *in vivo* tagging and pulldown of PI3K components (Tsolakos *et al*, 2018) suggest that monomeric p85α can be seen *in vivo* in some tissues.

We now address mechanisms underlying human mixed gain- and loss-of function phenotypes observed in association with PIK3R1 mutations using primary cells, cell models and in vitro enzyme assay and suggest that they are explained by competing effects of APDS2 PIK3R1 mutations on PI3K activity and stability.

Results

PI3K subunit expression and signalling in APDS2 fibroblasts

Disorders in the *PIK3CA*-related overgrowth spectrum (PROS) feature soft tissue overgrowth and are caused by mosaic activating mutations in *PIK3CA*, encoding the p110α catalytic subunit of PI3Kα(Madsen *et al*, 2018). In this group, basal hyperactivation of PI3Kα signalling can be easily discerned in dermal fibroblasts from affected areas of the body(Lindhurst *et al*, 2012). *PIK3R1*, like *PIK3CA*, is ubiquitously expressed, yet overgrowth is not reported in APDS2 caused by constitutional activating mutations in *PIK3R1*. Dermal fibroblasts strongly express *PIK3R1*, but no studies to date have evaluated whether PI3K activity is increased in APDS2.

We began by assessing dermal fibroblasts cultured from a previously described woman with APDS2 due to the common causal PIK3R1 mutation in the splice donor site that causes skipping of exon 11 and an in-frame deletion in the inter-SH2 domain shared by all PIK3R1 isoforms (Patient A.1 in (Lucas *et al.*, 2014b)). These cells were compared to cells from healthy control volunteers, or from people with PROS. Confirmation of expression of all pathogenic mutations was undertaken by cDNA sequencing prior to further study (**Fig 1**

supplement 1A). We found that truncated p85α was expressed, but at a much lower level than full length wild-type p85α (**Fig 1A, Fig 1 supplement 1B,C**). Despite this, no increase in basal or insulin-stimulated AKT phosphorylation was seen in APDS2 cells compared to cells from wild-type volunteers or from people with PROS and activating *PIK3CA* mutations H1047L or H1047R (**Fig 1A-C, Fig 1 supplement 2A,B**). Indeed, insulin-induced phosphorylation of AKT was lower in fibroblasts from this APDS2 patient compared to controls.

Previous studies have suggested that the truncated, APDS2-causal p85α variant exerts a much greater activating effect on p110δ, which has a more restricted tissue expression, including immune cells, than p110α, which is ubiquitous (Dornan *et al.*, 2017). We found that both p110α and p110δ were easily detectable in control dermal fibroblasts, however p110δ was almost absent in APDS2 fibroblasts compared to controls, with lower levels also seen in PROS cells (**Fig 1A,D, Fig 1 supplement 2D**). p110α was unchanged in APDS2 cells but modestly increased in PROS cells (**Fig 1A,E, Fig 1 supplement 2C**). Collectively these findings suggest that any ability of the APDS2 PIK3R1 variant in skin cells to activate PI3K may be overcome by reduced protein levels of p110δ, likely through reduced binding and/or reduced stabilisation of p110δ by the mutant regulatory subunit.

Overexpressed PIK3R1 ΔExon11 is potently dominant negative in 3T3-L1 preadipocytes

We next turned to a well-established cellular system allowing conditional overexpression of *PK3R1* alleles of interest. We have previously shown that overexpression of two SHORT syndrome PIK3R1 variants – R649W and Y657X – impair insulin signalling and adipocyte differentiation of murine 3T3-L1 preadipocytes, consistent with impaired PI3Kα function and with the lipodystrophy and insulin resistance seen in SHORT syndrome (Huang-Doran *et al*, 2016). To assess the effect of the APDS2 ΔEx11 in the same, non-immunological, cell context, we used lentiviral vectors, as previously described (Huang-Doran *et al.*, 2016), to generate clonal 3T3-L1 cell lines allowing conditional, tuneable overexpression of PIK3R1

variants in response to doxycycline. For signalling studies, we also generated cells conditionally overexpressing the PROS- and cancer-associated PIK3CA H1047R mutation as a positive control for increased PI3Kα signalling, while for differentiation studies we used previously reported lines conditionally expressing PIK3R1 R649W or Y657X (Huang-Doran *et al.*, 2016).

In undifferentiated cells, we first confirmed doxycycline-dependent overexpression of p85α or p110α transgenes (**Fig 2A**), before assessing basal and insulin-stimulated Akt phosphorylation. As expected, overexpression of oncogenic H1047R p110α strongly increased basal Akt phosphorylation (**Fig 2A-C, Fig 2 supplement 1A,C**) with no additional increase on insulin stimulation (**Fig 2A-C, Fig 2 supplement 1B,D**). Surprisingly, however, not only did overexpression of the APDS2 ΔEx11 p85α not increase basal PI3Kα signalling, but it potently inhibited insulin-induced Akt phosphorylation, consistent with a strong dominant negative action on pathway activation (**Fig 2A-C, Fig 2 supplement 1**). Overexpressing wild-type p85α mildly reduced insulin-stimulated Akt phosphorylation (**Fig 2A-C, Fig 2 supplement 1B,C**), although WT p85α was not expressed to as high a level as ΔEx11 p85α. In keeping with impaired PI3Kα activity, overexpression of the ΔEx11 variant also severely impaired adipocyte differentiation, assessed by triglyceride accumulation in response to a standard differentiation protocol (**Fig 2D**). A similar effect was seen on overexpressing SHORT syndrome variants R649W and Y657X (**Fig 2D**).

To assess whether the inhibitory effect of ΔEx11 p85α might be an artefact caused by strong overexpression, doxycycline titration was used to assess whether a low level of overexpression might unmask signalling hyperactivation. However, no such hyperactivation was seen, and instead, a graded diminution of insulin-induced AKT phosphorylation was observed from the lowest to highest levels of p85α ΔEx11 overexpression (**Fig 2 supplement 2**).

Effect of PIK3R1 mutations on Phosphoinositide 3-kinase activity in vitro

Given this evidence that APDS2-associated PIK3R1 ΔEx11 potently inhibits PI3Kα when overexpressed in 3T3-L1 preadipocytes, we next sought to investigate the biochemical basis of this observation. First, we assessed the effect of disease-causing PIK3R1 mutations on basal and phosphotyrosine-stimulated activity of purified PI3Kα, β and δ holoenzyme in a previously described reconstituted *in vitro* system(Burke *et al*, 2012). As well as the APDS2 ΔEx11 mutation, we selected three SHORT syndrome-associated mutations to study. These were the most common causal mutation, R649W, which abolishes phosphotyrosine binding by the C-terminal SH2 (cSH2) domain (Chudasama *et al.*, 2013), Y657X, which truncates the cSH2 domain (Huang-Doran *et al.*, 2016; Kwok *et al*, 2020), and E489K which, atypically, lies in the inter-SH2 domain where most cancer, overgrowth and APDS2-associated mutations lie (Thauvin-Robinet *et al.*, 2013). PIK3R1 E489K-containing primary cells were previously suggested to show basal hyperactivation (Thauvin-Robinet *et al.*, 2013).

Wild-type and SHORT syndrome mutant holoenzymes were successfully purified for *in vitro* assay, but despite multiple attempts, ΔEx11 holoenzyme could only be made in small amounts under identical conditions, and moreover was unstable on storage, precluding further study. In keeping with previous reports (Chudasama *et al.*, 2013; Dornan *et al.*, 2017; Dornan *et al*, 2020), p85α R649W showed severely reduced phosphotyrosine-stimulated activity in complex with p110α, with highly significant but lesser loss of function seen for Y657X and E489K (**Fig 3A, Fig 3 supplement 1A**). No increase in basal activity was seen for any variant.

We also assessed whether any of the SHORT syndrome variants affect function of PI3Kβ and found that all variants impaired phosphotyrosine-stimulated activity of PI3Kβ. Again, this impairment was less for p85α Y657X than for R649W, and in this case only very mild for E489K (**Fig 3B, Fig 3 supplement 1B**). For PI3Kδ, p85α R649W conferred severe loss of function, as for other isoforms (**Fig 3C, Fig 3 supplement 1C**), suggesting that the absence

of immunodeficiency in SHORT syndrome is not accounted for by selective inhibition of PI3Kα function by causal mutations.

Binding of p110α by mutant p85α

Given the potent dominant negativity of APDS2-related p85α ΔEx11 in cells, and the instability of p85α ΔEx11-containing PI3K holoenzyme *in vitro*, we next used immunoprecipitation to assess binding of p110α by this and other p85α variants in cells. p85α was easily detected in anti-p110α immunoprecipitates from all cell lines at baseline (**Fig 4**). No increase was seen on conditional overexpression of wild-type or R649W p85α. Given the known instability of monomeric p110α, this suggests that all p110α is bound to p85α before overexpression. Although wild-type endogenous p85α may have been replaced by heterologously overexpressed p85α in these cells, this could not be detected without a size difference of the variant from wild-type. For cells overexpressing the SHORT syndrome-associated p85α Y657X, the truncated variant was strongly co-immunoprecipitated, accounting for nearly all of the p85α signal in anti-p110α immunoprecipitate. This demonstrates preserved binding of p110α by mutant p85α (**Fig 4**). In sharp contrast, although truncated p85α ΔEx11 was easily detected in cell lysates before immunoprecipitation and in supernatant after immunoprecipitation (arrowed in **Fig 4**), no truncated p85α ΔEx11 was seen in p110α immunoprecipitates, and no change in p110α expression was detected (**Fig 4**). This suggests that this truncated APDS2 causal variant does not supplant endogenous, full-length p85α binding to p110α, despite overexpression. This argues against destabilisation of p110α as the mechanism of the observed dominant negative activity.

Effect of PIK3R1 mutations on insulin-induced PI3K recruitment to IRS1/2

As APDS2 p85α ΔEx11 does not appear to displace wild-type p85α from p110α, despite strong overexpression, it is likely that there are high levels of the monomeric truncated p85α in the cell. This may be important as it is p85α that mediates recruitment of PI3K to activated tyrosine kinase receptors and their tyrosine phosphorylated substrates, including the insulin-receptor substrate proteins Irs1 and Irs2. Excess free regulatory subunits compete with heterodimeric PI3K holenzyme (Ueki *et al.*, 2002), raising the possibility that excess free, truncated APDS2 p85α ΔEx11 may exert its inhibitory action by competing with PI3K holenzyme.

To assess this possibility, we again used the 3T3-L1 cellular model to determine whether overexpression of disease-causing p85α variants impairs recruitment of p110α to Irs1 and Irs2. Irs1 was immunoprecipitated with or without conditional p85α overexpression and with or without insulin stimulation. Overexpression of wild-type p85α had no effect on basal or insulin-induced p110α recruitment to Irs1 (**Fig 5A,B, Fig 5 supplement 1A,B**). In contrast, overexpression of either p85α R649W or Y657X sharply reduced insulin-stimulated p110α recruitment to Irs1 on insulin stimulation (**Fig 5A,B, Fig 5 supplement 1A,B**). In keeping with the inability of the R649W cSH2 domain to bind phosphotyrosines, p85α R649W was also not recruited to Irs1, while overexpression of Y657X increased stimulated but not basal p85α recruitment (**Fig 5A,C, Fig 5 supplement 1C,D**). This suggests a pure defect in PI3K holoenzyme recruitment for R649W. For Y657X the signalling defect may have mixed mechanisms, with reduced activation by phosphotyrosine seen in *in vitro* studies coupled to increased abundance of monomeric mutant p85α, leading to recruitment of non p110α-bound mutant p85α to Irs1.

In keeping with our finding of severely attenuated insulin signalling upon p85α ΔEx11 overexpression (**Fig 2**), overexpression of this mutant p85α abolished p110α recruitment to Irs1 (**Fig 5A,B, Fig 5 supplement 1A,B**). However, non p110α-bound p85α ΔEx11 was strongly recruited to Irs1 even in the absence of insulin stimulation (**Fig 5A,C, Fig 5 supplement 1C,D**). This suggests that although p85α ΔEx11 does not effectively compete

with wild-type p85α for binding to p110α, it has preserved or possibly enhanced ability to bind Irs1. This gives the mutant p85α properties that render it a more potent endogenous inhibitor of PI3K signalling than free wild-type p85α. Experiments conducted with immunoprecipitation of Irs2 instead of Irs1 yielded closely similar findings for all p85α species (**Fig 6 and Fig 6 supplement 1**).

Discussion

Murine genetic studies of Pik3r1 have proved complicated to interpret, due in part to functional redundancy among PI3K regulatory subunits, and in part to unanticipated effects of perturbing PI3K subunit stoichiometry. This has left several important questions about *in vivo* functions of Pik3r1 unresolved. Identification of a series of human genetic disorders caused by constitutional PIK3R1 mutations over the past 10 years has given fresh impetus to the field and has been mechanistically illuminating.

Homozygous truncating PIK3R1 mutations abolishing p85α expression while preserving p55α and p50α produce agammaglobulinaemia (Conley *et al*, 2012; Tang *et al*, 2018). This resembles the immunodeficiency reported in *Pik3r1* knockout mice (Fruman *et al*, 1999; Suzuki *et al*, 1999) and suggests an essential, non-redundant function of p85α in B cell development in humans. Thereafter, human genetics has provided more novel insights. *PIK3R1* mutations were identified in SHORT syndrome in 2013 (Chudasama *et al.*, 2013; Dyment *et al.*, 2013; Thauvin-Robinet *et al.*, 2013), nearly all in the C-terminal SH2 domain, which together with the N-terminal SH2 domain enables PI3K recruitment to activated RTKs (Rordorf-Nikolic *et al*, 1995). SHORT syndrome features short stature and insulin resistance consistent with impaired ligand-induced p110α action, a phenotype distinct from the enhanced insulin sensitivity produced by genetic ablation of one or more *Pik3r1* products in mice (Chen *et al.*, 2004; Fruman *et al.*, 2000; Mauvais-Jarvis *et al.*, 2002). Mice with SHORT syndrome mutations knocked in were generated after human findings, and faithfully reproduce the human phenotype (Kwok *et al.*, 2020; Solheim *et al*, 2018; Winnay *et al*,

2016), confirming that expression of a signalling-impaired PIK3R1 has different consequences to Pik3r1 knockout. No immunodeficiency has been described associated with classic SHORT syndrome mutations, however, suggesting a selective effect on PI3Kα, but the basis of this selectivity has not previously been investigated.

In contrast to SHORT syndrome, mutations in the inter SH2 domain of PIK3R1, mostly leading to skipping of exon 11, were shown in 2014 to activate PI3K *in vitro* and to cause immunodeficiency (APDS2) (Deau *et al.*, 2014; Lucas *et al.*, 2014b) similar to that caused by activating mutations in p110δ (APDS1) (Angulo *et al.*, 2013; Lucas *et al.*, 2014a). Neither overgrowth nor metabolic features of APDS2 have been described to suggest p110α hyperactivation, and indeed short stature is common in APDS2 (Elkaim *et al.*, 2016; Jamee *et al.*, 2020; Maccari *et al.*, 2023; Olbrich *et al.*, 2016; Petrovski *et al.*, 2016), with a growing number of APDS2 patients described with features of SHORT syndrome (Bravo Garcia-Morato *et al.*, 2017; Maccari *et al.*, 2023; Nguyen *et al.*, 2023; Petrovski *et al.*, 2016; Ramirez *et al.*, 2020; Szczawinska-Poplonyk *et al.*, 2022). Moreover mice with the common APDS2 causal Pik3r1 variant knocked in show impaired growth and *in utero* survival, unclike APDS2 murine models(Nguyen *et al.*, 2023).

Thus, study of distinct PIK3R1-related syndromes shows that impaired signalling caused by PIK3R1 mutations produces phenotypes related to impaired PI3Kα function, without affecting PI3Kδ. Conversely, mutations of PIK3R1 that produce phenotypes related to increased PI3Kδ signalling do not increase PI3Kα signalling. Indeed, they surprisingly have features characteristic of impaired PI3Kα function.

Lack of overgrowth in APDS2 has been attributed to greater ability of APDS2 PIK3R1 variants to activate p110δ than p110α (Dornan *et al.*, 2017), but the co-ocurrence of gain- and loss- of function phenotypes has not been explained to date. Our findings suggest that the explanation may lie in competing effects of APDS2 PIK3R1 variants to activate PI3Kδ on one hand, as previously shown (Angulo *et al.*, 2013; Dornan *et al.*, 2017; Lucas *et al.*,

2014b), while on the other hand interfering with PI3Kα through the dominant negative effect of non p110α-bound mutant p85α.

The low expression of truncated p85α ΔEx11 we described in dermal fibroblasts is similar to observations made in lymphocytes, however, in lymphocytes this is associated with increased basal AKT phosphorylation (Deau *et al.*, 2014; Lucas *et al.*, 2014b) that is abolished by p110δ inhibition (Lucas *et al.*, 2014b). P110δ is also expressed in fibroblasts, but protein levels were reduced in the cells studied, consistent with the previously reported observation that when expressed in insect cells the PI3K holoenzyme containing p85α ΔEx11 has a low yield and is unstable (Dornan *et al.*, 2017). We speculate that in cells with low endogenous p110δ protein expression, the destabilising effect of mutant PIK3R1 predominates over its activating effect.

The balance between expression and signalling may be a fine one, however, as transient overexpression of FLAG-tagged p85α ΔEx11 did increase AKT phosphorylation in 3T3 fibroblasts in a previous study, although expression of p110α, β and δ was not determined (Deau *et al.*, 2014). We find, in contrast, that overexpression of untagged p85α ΔEx11 has a strong inhibitory effect on insulin signalling, and we were unable to identify a window of overexpression where increased AKT phosphorylation could be observed. We further demonstrated that most or all of the mutant p85α expressed is not bound to p110α, while unbound mutant p85α still binds to Irs1/2, effectively competing with PI3K holoenzyme. The observation that p85α ΔEx11 can associate with Irs1/2 is in agreement with reports that p85α ΔEx11-containing PI3Kα and PI3Kδ can be stimulated by pY2-peptides (Dornan *et al.*, 2017; Dornan *et al.*, 2020) and that p85α ΔEx11 is recruited to tyrosine-phosphorylated LAT in T cells(Lucas *et al.*, 2014b). The competition we suggest between unbound mutant p85α and PI3K holoenzyme for binding to the activated RTKs is in keeping with longstanding evidence that free p85 downregulates PI3K signalling through the same competitive mechanism (Thorpe *et al*, 2017; Ueki *et al.*, 2002), with a single study suggesting in addition

that overexpression of tagged p85α leads to Irs1 sequestration with free p85α in cytosolic foci where PI(3,4,5)P3 production does not occur (Luo *et al*, 2005).

The current study has limitations. We have studied primary cells from only a single APDS2 patient, and in the 3T3-L1 cell model, we did not determine whether p110δ protein could be detected. If not, this could explain the lack of detectable AKT phosphorylation with induction of Pik3r1 ΔEx11. Our study moreover raises further questions. Full length p85α subunits can homodimerize (Cheung *et al*, 2015; Harpur *et al*, 1999; LoPiccolo *et al*, 2015), and it is speculated that homodimers may outcompete p85α/p110 heterodimers for binding to activated Irs1 due to configuration of the four SH2 domains. In the 3T3-L1 preadipocyte APDS2 models, p85α ΔEx11 expression was high despite impaired p110α association, but whether this is composed of monomeric or homodimeric p85α, and whether mutant p85α expression leads to sequestration of Irs1 remote from the insulin receptor, as previously suggested for tagged wild-type p85α, is undetermined.

In summary, it is already established that: A. genetic activation of PIK3CD causes immunodeficiency without disordered growth, while B. inhibition of PIK3R1 recruitment to RTKs and their substrates impairs growth and insulin action, without immunodeficiency, despite all catalytic subunits being affected and C. loss of p85α alone causes immunodeficiency. The current study, coupled with prior reports, suggests that the common APDS2 mutation in PIK3R1 has mixed consequences, producing greater hyperactivation of p110δ than p110α, based on subtle differences in the inhibitory interactions of regulatory and catalytic subunits, while also destabilising PI3K holoenzyme and exerting dominant negative activity on wild-type PIK3R1 function. We suggest that these competing activating and inhibitory consequences are finely balanced, potentially differing among tissues, leading to mixed clinical profiles of gain- and loss-of function features.

Materials and Methods

Ethics

The patient studied gave written informed consent for NIH IRB-approved research protocols 06-I-0015 and 09-I-0133 and was reported previously(Lucas *et al.*, 2014b). Dermal fibroblasts were isolated from a skin punch biopsy and cultured as previously described(Huang-Doran *et al.*, 2016).

Baculovirus Generation

p85α point mutation expression constructs were created by site-directed mutagenesis of a pACEBac1_Homo sapiens p85α plasmid using a QuikChange II XL Site-Directed Mutagenesis Kit. In-Fusion cloning was used to generate pACEBac1_p85α ΔEx11. In brief, pACEBac1_p85α backbone was digested (BamHI/NotI) and purified using Zymoclean Gel DNA Recovery Kit, while cDNA insert was purified using NucleoSpin® Clean-up Kit (Takara). Insert generation was performed by High-Fidelity PCR using primers designed to yield fragments containing exons 1-10 or 12-16 with the necessary overlap, with inserts verified by electrophoresis and purified using NucleoSpin® Clean-up kit. In-Fusion reactions were performed according to manufacturer's guideline (Takara) using 100ng each of linearised plasmid and both inserts in 10µL. Products were transformed into Stellar Competent cells (Takara). Purified plasmid inserts were sequenced and verified by restriction enzyme digest, exploiting loss of a DpnI site within excised exon 11.

pACEBac1_p85α and pFastBac™HT B plasmids encoding N terminally tandem His-tagged p110 subunits were used to generate bacmid DNA. MAX Efficiency DH10Bac™ Competent or EMBacY cells (Thermofisher) were transformed with 40ng plasmid DNA and turbid cultures plated onto agar containing 50µg/mL kanamycin, 10µg/mL gentamicin, 10µg/mL tetracycline, 100µg/mL X-Gal and 40µg/mL IPTG. Single colonies were picked, expanded and purified at 2 days and bacmid concentrations quantified by Nanodrop 1000 Spectrophotometer (Thermo Scientific). 2-4µg bacmid was transfected into Sf9 cells in 6 well plates using Insect-XPRESS (Promega E2311). Cells were incubated at 2°C for 5 days and bacmid YFP expression assessed by Leica DM IL LED Fluo microscope using a green fluorescent protein filter cube. Pooled virus from 2 wells of supernatant (P1 stock) was used

to produce high titre P2 stock by transfection of 1.5x106 Sf9 cells/mL (Thermofisher) in 450mL using Insect-XPRESS with L-Glutamine (Lonza LZBE12-730Q). For catalytic subunits, 1-2mL P2 stock was used for a further round of Sf9 transfection and expansion to generate P3 stock.

Purification of PI3K holoenzymes

1.5-2L of 1.5x106 Sf9 cells/mL were co-infected with 18mL P3 catalytic subunit and 4mL P2 regulatory subunit baculovirus. Non infected Sf9 cells were negative controls, and a prior protein preparation of 320 kDa was the positive control. Cells were cultured at 27°C, harvested 48h post-infection, pelleted, washed and stored at -80°C. Pellets were later lysed by sonication in buffer containing 20 mM TrisHCl (pH 8.0), 300 mM NaCl, 20 mM imidazole (pH 8.0) and 1 mM TCEP (pH 7.0) at 4 °C. Universal Nuclease (Thermofisher) was added to lysates before ultracentrifugation at 35,000 rpm for 35min at 4°C. p85α/p110 heterodimers were pulled down via 6 tandem p110 N-terminal His tags, preventing purification of monomeric p85α, using tandem Ni2+HisTrap Fast Flow columns (GE Healthcare) (equilibration buffer 20 mM TrisHCl (pH 8.0), 100 mM NaCl, 20 mM imidazole and 1 mM TCEP (pH 7.0); elution buffer 20 mM TrisHCl (pH 8.0), 100 mM NaCl, 200 mM imidazole and 1 mM TCEP (pH 7.0)). Further purification utilised a heparin HiTrap Q HP column (GE Healthcare) equilibrated with 20mM TrisHCl (pH 8.0) and 1mM TCEP (pH 7.0), with proteins eluted in 20mM TrisHCl (pH 8.0), 1 M NaCl and 1mM TCEP (pH 7.0). Eluted fractions were concentrated to ≥1mg/mL using Millipore Amicon Ultra-15 Centrifugal Filter Units with Ultracel-50 membrane, and 1mL concentrated fractions were gel filtered on Superdex 200 16/60 columns (GE Healthcare) equilibrated in 20mM HEPES (pH 7.5), 100mM NaCl and 2mM TCEP (pH 7.0). The p110 6-His tag was retained for proteins used in functional analyses. KTA Protein Purification Systems (GE Healthcare) and UNICORN Control Software version 5.11 (GE Healthcare) were used for all purifications. Purity of eluted complexes was verified by SDS-PAGE, and purified proteins were quantified using a Nanodrop 1000 Spectrophotometer (Thermofisher). Protein concentration was calculated using the molecular extinction coefficient (assuming full cysteine reduction) determined by

heterodimer sequence input to the ProtParam tool (ExPASy). Purified proteins were stored at –80°C in single-use aliquots.

Total injection volume onto gel filtration columns was kept at 1 mL. Yields of PI3K complexes were determined using the area under the curve (280nm mAU per mL eluted protein) from gel filtration chromatograms, and normalised to the volume of Sf9 cells infected.

Liposome preparation

Chloroform/methanol solutions of sphingomyelin, cholesterol, porcine brain phosphatidylcholine, porcine brain phosphatidylethanolamine, porcine brain phosphatidylserine and porcine brain PI(4,5)P2 were mixed to generate a preparation containing 5/10/15/45/20/5% of each lipid, with a total lipid concentration of 5 mg/mL and final PI(4,5)P2 concentration 250µg/mL. Lipid preparations were dessicated under argon and then in a vacuum desiccator. Lipids were rehydrated in buffer containing 20mM HEPES (pH 7.5), 100 mM KCl and 1 mM EGTA (pH 8.0) using vortexing for 3 min, waterbath sonication for 15 min, and 10 cycles between liquid nitrogen and a 43°C water bath. Unilamellar vesicles were generated by extrusion through polycarbonate filters with 100nm pores, using a glass-tight syringe. Single use aliquots were stored at -80 °C.

Fluorescence Polarisation Assay

PI(3,4,5)P3 production was measured by modified PI3-Kinase activity fluorescence polarisation assay (Echelon Biosciences, Salt Lake City, UT, USA). 10µL reactions in 384-well black microtitre plates used 1mM liposomes containing 50µM PI(4,5)P2, optimised concentrations of purified PI3K proteins, 100µM ATP, 2mM MgCl2, with or without 1µM tyrosine bisphosphorylated peptide derived from PDGFRβ ("pY2"; Cambridge peptides). Reactions were quenched with 5µL of solution containing 20mM HEPES (pH 7.5), 150mM NaCl, 30mM EDTA (pH 7.4) and 400nM GST–Grp1-PH, followed by addition of 5µL 40nM TAMRA Red Fluorescent Probe in HNT buffer. Identity of the lipid group coupled to the TAMRA probe was not disclosed by Echelon Biosciences, but as Grp1 recognises specific lipid head groups in competition with PI(3,4,5)P3, it is likely to be a lipid with a similar head

group such as inositol 1,3,4,5-tetrakisphosphate. After 1h equilibration, fluorescence polarisation was measured using a PHERAstar spectrofluorometer (BMG Labtech, Ortenberg, Germany) with the FP/540-20/590-20/590-20 optical module. The concentrations of wild-type protein complexes used in the assay were: 20-40nM p85α/p110α, 80-160nM p85α/p110β and 80-160nM p85α/p110δ for basal activities, and 1-2nM p85α/p110α, 2-4 nM p85α/p110β and 2-6nM p85α/p110δ for pY2-stimulated activities. Concentrations of thawed protein aliquots were assessed as 280 nm absorbance by Nanodrop 1000 Spectrophotometer, and samples of preparations used in assays were resolved by SDS-PAGE to confirm equal amounts of each complex. Three technical replicates were used per assay on at least three different occasions. Relevant wild-type p85α/p110 catalytic isoforms were included in each assay as controls. Other controls were 1. Stop mix + probe without lipids, to assess maximum fluorescence polarisation. 2. Stop mix + probe with lipids, to determine the effect of lipids on maximum fluorescence polarisation. 3. Probe without stop mix or lipids to determine minimum fluorescence polarisation and 4. Probe with lipids but no stop mix to determine the effect of lipids on minimum fluorescence polarisation. Standard curves of diC8-PI(3,4,5)P3 in the presence of liposomes were included in every experiment and used to infer PIP3 generated by purified PI3K. Graphpad Prism v6.0 was used to generate sigmoidal standard curves by plotting log transformed diC8-PI(3,4,5)P3 concentrations against fluorescence polarisation. Standard curves for each experiment provided the linear range within which PIP3 could be accurately determined. Preliminary studies found only trivial differences in measured fluorescence polarisation in the presence of pY2, which was thus omitted from subsequent standard curves. Quadruplicate interpolated PIP3 concentrations were averaged and normalised by reaction time (30 min) and enzyme concentration in pM to yield PI3K activity in pmol PIP3/min/pM enzyme. Specific activities were then further normalised to activity of p85α wild-type controls in the presence of pY2 in each experiment.

Generation of 3T3-L1 cells conditionally expressing p85α or p110α

3T3-L1 preadipocytes from Zenbio were cultured, differentiated and stained for neutral lipid with Oil Red O as previously described(Huang-Doran *et al*, 2011). Generation of 3T3-L1 sublines inducibly expressing WT, Y657X, or R649W p85α was also previously reported(Huang-Doran *et al.*, 2016; Hussain *et al*, 2011). The 3T3-L1 lines inducibly expressing p85α ΔEx11 or p110α H1047R were generated using essentially the same procedure, starting with In-Fusion subcloning of the p85α ΔEx11 cDNA insert from the pACEBac1 p85α ΔEx11 plasmid described above, and of a PIK3CA H1047R cDNA insert derived by PCR from a pcDNA5.FRT.Teton_FLAG_PIK3CA-H1047R plasmid, into the pEN_Tmcs entry vector. Transgene expression was induced with 1 µg/mL doxycycline for 72 hours.

Insulin signalling studies

3T3-L1 cells serum starved in DMEM containing 0.5 % BSA for 16h were stimulated with 100nM Actrapid insulin (Novo Nordisk) for 10min. Monolayers were snap frozen in liquid N2 and stored at -80°C. 200-600µL co-IP lysis (20mM HEPES, 150mM NaCl, 1.5mM MgCl2, 10% (v/v) glycerol, 1% (v/v) Triton X-100, 1mM EGTA pH 7.4, 1mM PMSF, 2mM activated sodium orthovanadate, Complete Mini EDTA-free protease inhibitor cocktail and PhosSTOP, in Milli-Q Ultrapure water (Millipore)) or RIPA buffer (50mM Tris HCl pH 8.0, 150mM NaCl, 1% NP-40, 0.5% sodium deoxycholate, 0.1% SDS with added Complete Mini EDTA-free protease inhibitor cocktail and PhosSTOP, in Milli-Q Ultrapure Water (Millipore)) was added to frozen cells before scraping of lysate into pre-chilled tubes, incubation on ice for 30min and clearing by centrifugation. Protein was quantified using the Bio-Rad DC assay.

Lysates were mixed with NuPAGE® SDS Loading buffer supplemented with 5% □-mercaptoethanol and boiled before SDS-PAGE. For co-immunoprecipitation (Co-IP) lysates (150-300µg protein) were incubated in 500µL Co-IP buffer with immunoprecipitating antibody overnight at 4°C. 10µg lysate mixed with NuPAGE® SDS Loading buffer and 5% □-mercaptoethanol was stored to represent Co-IP input. Co-IP samples were incubated for 2h with 1.5mg PBST-washed Protein G Dynabeads® (Life Technologies) at 4°C before

centrifugation and bead removal using a DynaMag™-2 Magnet (Invitrogen). Supernatants mixed 1:1 with Co-IP elution buffer (2X NuPAGE® LDS, 100 mM NuPAGE® Sample Reducing Agent, in Co-IP lysis buffer) were boiled for 10 min. Beads were washed 5 times in 50µL Co-IP lysis buffer, before protein elution with 25µL Co-IP Elution buffer and boiling for 10min. Input, supernatant and co-IP samples underwent SDS-PAGE using NuPAGE® 4-12% gradient Bis-Tris gels in NuPAGE® MOPS SDS Running Buffer. Transfer to nitrocellulose was performed using the iBlot™ Dry Blotting System (Invitrogen), with preincubation in Equilibration Transfer Buffer for proteins above 150kDa.

For immunoblotting, blocked membranes were incubated overnight at 4°C in primary antibody, washed and incubated with HRP-linked anti-rabbit or anti-mouse IgG secondary antibody diluted 1:5000 in blocking buffer. Proteins were visualized using the ChemiDoc™ MP System (Bio-Rad) and band intensities quantified using Image Lab software (Bio-Rad).

Statistical Analysis

For quantitative data, all biological replicates (i.e. results of independent experiments on different days) are represented in figures, with paired points (e.g. with/without insulin in the same experiment) connected by lines. For fluorescence polarisation assays, each biological replicate shown is the mean of 3 technical replicates. Sample size for individual experiments was not pre-determined. To avoid the pitfalls of dichotomous significance testing on low-throughput biological datasets, we used estimation statistics (Data Analysis using Bootstrap-Coupled ESTimation) with default settings (5000 resamples, BCa boostrap)(Ho *et al*, 2019). This focuses on effect sizes and derives confidence intervals derived from bootstrapping for differences in means; the small (but typical) sample size of the experiments analysed limits reliable bootstrapping, but it offers additional confidence to the consistent patterns seen in independent replicates. We have indicated significance in main text figures with an asterisk, and show the 95% confidence intervals for mean differences in extended view figures.

All antibodies used are listed in **Table 1**.

Data Availability

This study includes no data deposited in external repositories. Uncut Western blot and other source images are available on the Open Science Framework project webpage: https://osf.io/eyc4h/?view_only=9af8645c8fe5408790ce19920d0084c6.

Acknowledgements

This work was supported by the Wellcome Trust through a grant to RKS [210752/Z/18/Z] and a studentship to PRT [102356/Z/13/Z]. Additional support was from the UK Medical Research Council (MRC) [MC_UU_12012/5 and MC_U105184308 (to RLW)] and the Intramural Research Program of the National Institute of Allergy and Infectious Diseases, National Institutes of Health (to HCS). We thank Dr. Koneti Rao, Debra Long-Priel, and Angela Wang for clinical, technical, and regulatory assistance.

Author Contributions

PRT: conceptualisation, methodology, formal analysis, investigation, visualization, writing - original draft. **RK**: formal analysis, investigation, visualization. **OP**: supervision, methodology, investigation, writing - review & editing. **HCS:** resources, funding acquisition, writing - review & editing. **GVB:** supervision, methodology, writing - review & editing. **RLW**: supervision, methodology, investigation, funding acquisition, writing - review & editing. **RKS:** conceptualisation, supervision, methodology, funding acquisition, writing - original draft, writing - review & editing, funding acquisition.

Disclosure and competing interests statement

RKS has consulted for Novartis on clinical aspects of PIK3CA-related overgrowth, and for Alnylam, Amryt and AstraZeneca on clinical aspects of monogenic insulin resistance and lipodystrophy

References

562 Angulo I, Vadas O, Garcon F, Banham-Hall E, Plagnol V, Leahy TR, Baxendale H, Coulter T,
563 Curtis J, Wu C *et al* (2013) Phosphoinositide 3-kinase delta gene mutation predisposes to
564 respiratory infection and airway damage. *Science* 342: 866-871
565 Avila M, Dyment DA, Sagen JV, St-Onge J, Moog U, Chung BHY, Mo S, Mansour S, Albanese
566 A, Garcia S *et al* (2016) Clinical reappraisal of SHORT syndrome with PIK3R1 mutations:
567 toward recommendation for molecular testing and management. *Clin Genet* 89: 501-506
568 Brachmann SM, Ueki K, Engelman JA, Kahn RC, Cantley LC (2005) Phosphoinositide 3-kinase
569 catalytic subunit deletion and regulatory subunit deletion have opposite effects on insulin
570 sensitivity in mice. *Mol Cell Biol* 25: 1596-1607
571 Bravo Garcia-Morato M, Garcia-Minaur S, Molina Garicano J, Santos Simarro F, Del Pino
572 Molina L, Lopez-Granados E, Ferreira Cerdan A, Rodriguez Pena R (2017) Mutations in
573 PIK3R1 can lead to APDS2, SHORT syndrome or a combination of the two. *Clin Immunol* 179:
574 77-80
575 Burke JE, Perisic O, Masson GR, Vadas O, Williams RL (2012) Oncogenic mutations mimic
576 and enhance dynamic events in the natural activation of phosphoinositide 3-kinase
577 p110alpha (PIK3CA). *Proc Natl Acad Sci U S A* 109: 15259-15264
578 Chen D, Mauvais-Jarvis F, Bluher M, Fisher SJ, Jozsi A, Goodyear LJ, Ueki K, Kahn CR (2004)
579 p50alpha/p55alpha phosphoinositide 3-kinase knockout mice exhibit enhanced insulin
580 sensitivity. *Mol Cell Biol* 24: 320-329
581 Cheung LW, Walkiewicz KW, Besong TM, Guo H, Hawke DH, Arold ST, Mills GB (2015)
582 Regulation of the PI3K pathway through a p85alpha monomer-homodimer equilibrium. *Elife*
583 4: e06866
584 Chudasama KK, Winnay J, Johansson S, Claudi T, Konig R, Haldorsen I, Johansson B, Woo JR,
585 Aarskog D, Sagen JV *et al* (2013) SHORT syndrome with partial lipodystrophy due to
586 impaired phosphatidylinositol 3 kinase signaling. *Am J Hum Genet* 93: 150-157
587 Conley ME, Dobbs AK, Quintana AM, Bosompem A, Wang YD, Coustan-Smith E, Smith AM,
588 Perez EE, Murray PJ (2012) Agammaglobulinemia and absent B lineage cells in a patient
589 lacking the p85alpha subunit of PI3K. *J Exp Med* 209: 463-470
590 Cottrell CE, Bender NR, Zimmermann MT, Heusel JW, Corliss M, Evenson MJ, Magrini V,
591 Corsmeier DJ, Avenarius M, Dudley JN *et al* (2021) Somatic PIK3R1 variation as a cause of
592 vascular malformations and overgrowth. *Genet Med*
593 Deau MC, Heurtier L, Frange P, Suarez F, Bole-Feysot C, Nitschke P, Cavazzana M, Picard C,
594 Durandy A, Fischer A *et al* (2014) A human immunodeficiency caused by mutations in the
595 PIK3R1 gene. *J Clin Invest* 124: 3923-3928
596 Dornan GL, Siempelkamp BD, Jenkins ML, Vadas O, Lucas CL, Burke JE (2017)
597 Conformational disruption of PI3Kdelta regulation by immunodeficiency mutations in
598 PIK3CD and PIK3R1. *Proc Natl Acad Sci U S A* 114: 1982-1987
599 Dornan GL, Stariha JTB, Rathinaswamy MK, Powell CJ, Boulanger MJ, Burke JE (2020)
600 Defining How Oncogenic and Developmental Mutations of PIK3R1 Alter the Regulation of
601 Class IA Phosphoinositide 3-Kinases. *Structure* 28: 145-156 e145
602 Dyment DA, Smith AC, Alcantara D, Schwartzentruber JA, Basel-Vanagaite L, Curry CJ,
603 Temple IK, Reardon W, Mansour S, Haq MR *et al* (2013) Mutations in PIK3R1 cause SHORT
604 syndrome. *Am J Hum Genet* 93: 158-166
605 Elkaim E, Neven B, Bruneau J, Mitsui-Sekinaka K, Stanislas A, Heurtier L, Lucas CL, Matthews
606 H, Deau MC, Sharapova S *et al* (2016) Clinical and immunologic phenotype associated with
607 activated phosphoinositide 3-kinase delta syndrome 2: A cohort study. *J Allergy Clin*
608 *Immunol* 138: 210-218 e219

609 Fruman DA, Chiu H, Hopkins BD, Bagrodia S, Cantley LC, Abraham RT (2017) The PI3K
610 Pathway in Human Disease. *Cell* 170: 605-635
611 Fruman DA, Mauvais-Jarvis F, Pollard DA, Yballe CM, Brazil D, Bronson RT, Kahn CR, Cantley
612 LC (2000) Hypoglycaemia, liver necrosis and perinatal death in mice lacking all isoforms of
613 phosphoinositide 3-kinase p85 alpha. *Nat Genet* 26: 379-382
614 Fruman DA, Snapper SB, Yballe CM, Davidson L, Yu JY, Alt FW, Cantley LC (1999) Impaired B
615 cell development and proliferation in absence of phosphoinositide 3-kinase p85alpha.
616 *Science* 283: 393-397
617 Geering B, Cutillas PR, Nock G, Gharbi SI, Vanhaesebroeck B (2007) Class IA
618 phosphoinositide 3-kinases are obligate p85-p110 heterodimers. *Proc Natl Acad Sci U S A*
619 104: 7809-7814
620 Harpur AG, Layton MJ, Das P, Bottomley MJ, Panayotou G, Driscoll PC, Waterfield MD (1999)
621 Intermolecular interactions of the p85alpha regulatory subunit of phosphatidylinositol 3-
622 kinase. *J Biol Chem* 274: 12323-12332
623 Ho J, Tumkaya T, Aryal S, Choi H, Claridge-Chang A (2019) Moving beyond P values: data
624 analysis with estimation graphics. *Nat Methods* 16: 565-566
625 Huang-Doran I, Bicknell LS, Finucane FM, Rocha N, Porter KM, Tung YC, Szekeres F, Krook A,
626 Nolan JJ, O'Driscoll M *et al* (2011) Genetic defects in human pericentrin are associated with
627 severe insulin resistance and diabetes. *Diabetes* 60: 925-935
628 Huang-Doran I, Tomlinson P, Payne F, Gast A, Sleigh A, Bottomley W, Harris J, Daly A, Rocha
629 N, Rudge S *et al* (2016) Insulin resistance uncoupled from dyslipidemia due to C-terminal
630 PIK3R1 mutations. *JCI Insight* 1: e88766
631 Hussain K, Challis B, Rocha N, Payne F, Minic M, Thompson A, Daly A, Scott C, Harris J,
632 Smillie BJ *et al* (2011) An activating mutation of AKT2 and human hypoglycemia. *Science*
633 334: 474
634 Jamee M, Moniri S, Zaki-Dizaji M, Olbrich P, Yazdani R, Jadidi-Niaragh F, Aghamahdi F,
635 Abolhassani H, Condliffe AM, Aghamohammadi A *et al* (2020) Clinical, Immunological, and
636 Genetic Features in Patients with Activated PI3Kdelta Syndrome (APDS): a Systematic
637 Review. *Clin Rev Allergy Immunol* 59: 323-333
638 Kwok A, Zvetkova I, Virtue S, Luijten I, Huang-Doran I, Tomlinson P, Bulger DA, West J,
639 Murfitt S, Griffin J *et al* (2020) Truncation of Pik3r1 causes severe insulin resistance
640 uncoupled from obesity and dyslipidaemia by increased energy expenditure. *Mol Metab* 40:
641 101020
642 Lindhurst MJ, Parker VE, Payne F, Sapp JC, Rudge S, Harris J, Witkowski AM, Zhang Q,
643 Groeneveld MP, Scott CE *et al* (2012) Mosaic overgrowth with fibroadipose hyperplasia is
644 caused by somatic activating mutations in PIK3CA. *Nat Genet* 44: 928-933
645 LoPiccolo J, Kim SJ, Shi Y, Wu B, Wu H, Chait BT, Singer RH, Sali A, Brenowitz M, Bresnick AR
646 *et al* (2015) Assembly and Molecular Architecture of the Phosphoinositide 3-Kinase
647 p85alpha Homodimer. *J Biol Chem* 290: 30390-30405
648 Lucas CL, Kuehn HS, Zhao F, Niemela JE, Deenick EK, Palendira U, Avery DT, Moens L,
649 Cannons JL, Biancalana M *et al* (2014a) Dominant-activating germline mutations in the gene
650 encoding the PI(3)K catalytic subunit p110delta result in T cell senescence and human
651 immunodeficiency. *Nat Immunol* 15: 88-97
652 Lucas CL, Zhang Y, Venida A, Wang Y, Hughes J, McElwee J, Butrick M, Matthews H, Price S,
653 Biancalana M *et al* (2014b) Heterozygous splice mutation in PIK3R1 causes human
654 immunodeficiency with lymphoproliferation due to dominant activation of PI3K. *J Exp Med*
655 211: 2537-2547

656 Luo J, Field SJ, Lee JY, Engelman JA, Cantley LC (2005) The p85 regulatory subunit of
657 phosphoinositide 3-kinase down-regulates IRS-1 signaling via the formation of a
658 sequestration complex. *J Cell Biol* 170: 455-464
659 Maccari ME, Wolkewitz M, Schwab C, Lorenzini T, Leiding JW, Aladjdi N, Abolhassani H,
660 Abou-Chahla W, Aiuti A, Azarnoush S *et al* (2023) Activated phosphoinositide 3-kinase delta
661 syndrome: Update from the ESID Registry and comparison with other autoimmune-
662 lymphoproliferative inborn errors of immunity. *J Allergy Clin Immunol* 152: 984-996 e910
663 Madsen RR, Vanhaesebroeck B, Semple RK (2018) Cancer-Associated PIK3CA Mutations in
664 Overgrowth Disorders. *Trends Mol Med* 24: 856-870
665 Mauvais-Jarvis F, Ueki K, Fruman DA, Hirshman MF, Sakamoto K, Goodyear LJ, Iannacone M,
666 Accili D, Cantley LC, Kahn CR (2002) Reduced expression of the murine p85alpha subunit of
667 phosphoinositide 3-kinase improves insulin signaling and ameliorates diabetes. *J Clin Invest*
668 109: 141-149
669 Nguyen T, Lau A, Bier J, Cooke KC, Lenthall H, Ruiz-Diaz S, Avery DT, Brigden H, Zahra D,
670 Sewell WA *et al* (2023) Human PIK3R1 mutations disrupt lymphocyte differentiation to
671 cause activated PI3Kdelta syndrome 2. *J Exp Med* 220
672 Olbrich P, Lorenz M, Cura Daball P, Lucena JM, Rensing-Ehl A, Sanchez B, Fuhrer M,
673 Camacho-Lovillo M, Melon M, Schwarz K *et al* (2016) Activated PI3Kdelta syndrome type 2:
674 Two patients, a novel mutation, and review of the literature. *Pediatr Allergy Immunol* 27:
675 640-644
676 Petrovski S, Parrott RE, Roberts JL, Huang H, Yang J, Gorentla B, Mousallem T, Wang E,
677 Armstrong M, McHale D *et al* (2016) Dominant Splice Site Mutations in PIK3R1 Cause Hyper
678 IgM Syndrome, Lymphadenopathy and Short Stature. *J Clin Immunol* 36: 462-471
679 Philp AJ, Campbell IG, Leet C, Vincan E, Rockman SP, Whitehead RH, Thomas RJ, Phillips WA
680 (2001) The phosphatidylinositol 3'-kinase p85alpha gene is an oncogene in human ovarian
681 and colon tumors. *Cancer Res* 61: 7426-7429
682 Ramirez L, Tamayo W, Ale H (2020) APDS2 and SHORT Syndrome in a Teenager with PIK3R1
683 Pathogenic Variant. *J Clin Immunol* 40: 1020-1025
684 Rordorf-Nikolic T, Van Horn DJ, Chen D, White MF, Backer JM (1995) Regulation of
685 phosphatidylinositol 3'-kinase by tyrosyl phosphoproteins. Full activation requires
686 occupancy of both SH2 domains in the 85-kDa regulatory subunit. *J Biol Chem* 270: 3662-
687 3666
688 Solheim MH, Winnay JN, Batista TM, Molven A, Njolstad PR, Kahn CR (2018) Mice Carrying a
689 Dominant-Negative Human PI3K Mutation Are Protected From Obesity and Hepatic
690 Steatosis but Not Diabetes. *Diabetes* 67: 1297-1309
691 Suzuki H, Terauchi Y, Fujiwara M, Aizawa S, Yazaki Y, Kadowaki T, Koyasu S (1999) Xid-like
692 immunodeficiency in mice with disruption of the p85alpha subunit of phosphoinositide 3-
693 kinase. *Science* 283: 390-392
694 Szczawinska-Poplonyk A, Bernat-Sitarz K, Schwartzmann E, Piechota M, Badura-Stronka M
695 (2022) Clinical and immunological assessment of APDS2 with features of the SHORT
696 syndrome related to a novel mutation in PIK3R1 with reduced penetrance. *Allergol*
697 *Immunopathol (Madr)* 50: 1-9
698 Tang P, Upton JEM, Barton-Forbes MA, Salvadori MI, Clynick MP, Price AK, Goobie SL (2018)
699 Autosomal Recessive Agammaglobulinemia Due to a Homozygous Mutation in PIK3R1. *J Clin*
700 *Immunol* 38: 88-95

701 Thauvin-Robinet C, Auclair M, Duplomb L, Caron-Debarle M, Avila M, St-Onge J, Le Merrer
702 M, Le Luyer B, Heron D, Mathieu-Dramard M *et al* (2013) PIK3R1 mutations cause syndromic
703 insulin resistance with lipoatrophy. *Am J Hum Genet* 93: 141-149
704 Thorpe LM, Spangle JM, Ohlson CE, Cheng H, Roberts TM, Cantley LC, Zhao JJ (2017) PI3K-
705 p110alpha mediates the oncogenic activity induced by loss of the novel tumor suppressor
706 PI3K-p85alpha. *Proc Natl Acad Sci U S A* 114: 7095-7100
707 Tsolakos N, Durrant TN, Chessa T, Suire SM, Oxley D, Kulkarni S, Downward J, Perisic O,
708 Williams RL, Stephens L *et al* (2018) Quantitation of class IA PI3Ks in mice reveals p110-free-
709 p85s and isoform-selective subunit associations and recruitment to receptors. *Proc Natl*
710 *Acad Sci U S A* 115: 12176-12181
711 Ueki K, Fruman DA, Brachmann SM, Tseng YH, Cantley LC, Kahn CR (2002) Molecular balance
712 between the regulatory and catalytic subunits of phosphoinositide 3-kinase regulates cell
713 signaling and survival. *Mol Cell Biol* 22: 965-977
714 Wentink M, Dalm V, Lankester AC, van Schouwenburg PA, Scholvinck L, Kalina T, Zachova R,
715 Sediva A, Lambeck A, Pico-Knijnenburg I *et al* (2017) Genetic defects in PI3Kdelta affect B-
716 cell differentiation and maturation leading to hypogammaglobulineamia and recurrent
717 infections. *Clin Immunol* 176: 77-86
718 Winnay JN, Solheim MH, Dirice E, Sakaguchi M, Noh HL, Kang HJ, Takahashi H, Chudasama
719 KK, Kim JK, Molven A *et al* (2016) PI3-kinase mutation linked to insulin and growth factor
720 resistance in vivo. *J Clin Invest* 126: 1401-1412
721 Yu J, Zhang Y, McIlroy J, Rordorf-Nikolic T, Orr GA, Backer JM (1998) Regulation of the
722 p85/p110 phosphatidylinositol 3'-kinase: stabilization and inhibition of the p110alpha
723 catalytic subunit by the p85 regulatory subunit. *Mol Cell Biol* 18: 1379-1387
724 Zhao JJ, Cheng H, Jia S, Wang L, Gjoerup OV, Mikami A, Roberts TM (2006) The p110alpha
725 isoform of PI3K is essential for proper growth factor signaling and oncogenic
726 transformation. *Proc Natl Acad Sci U S A* 103: 16296-16300
727

Figures

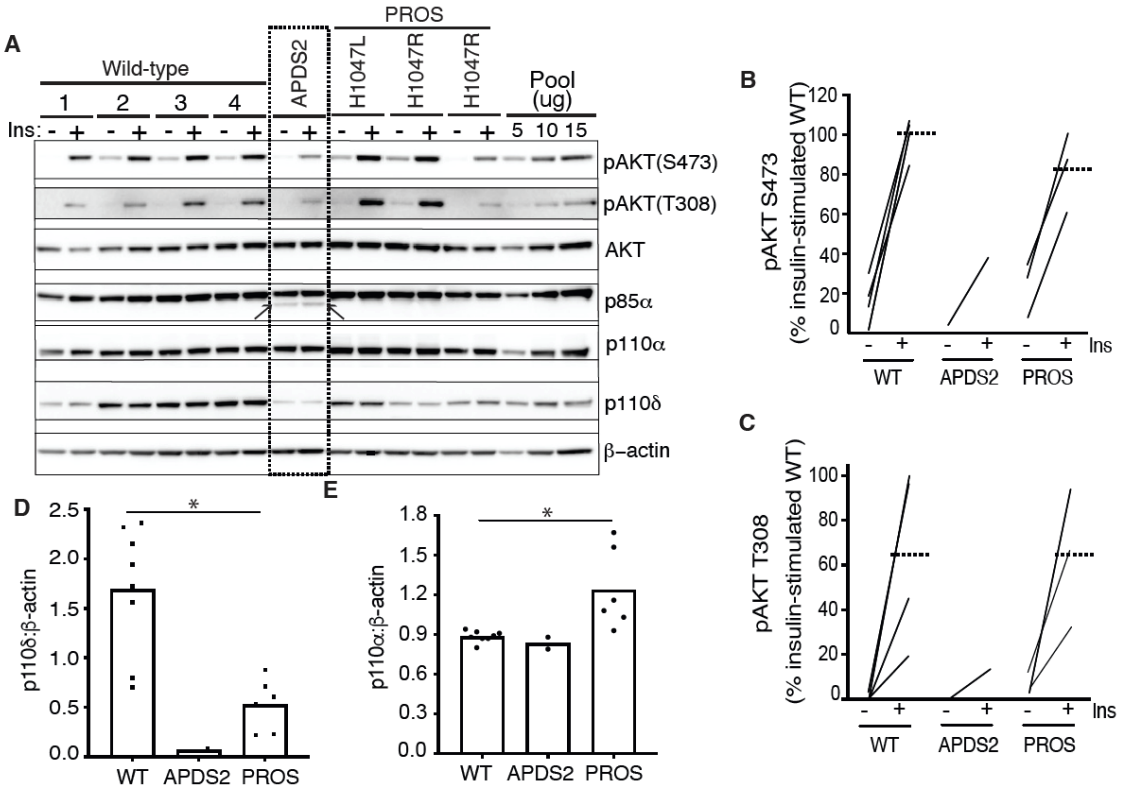

Figure 1. PI3K subunit expression and signalling in primary dermal fibroblasts. Immunoblotting of AKT, AKT phosphorylated at threonine 308 (T308) or serine 473 (S473), p85α, p110δ and p110α and are shown with and without stimulation by 100 nM insulin (Ins) for 10 minutes. β-actin is shown as a loading control, with different amounts of pooled lysate (Pool) used to demonstrate signal intensity in the linear range. Results from 4 healthy controls (WT; 1-4), 1 patient with Activating p110 Delta Syndrome 2 (APDS2) due to the p85α Δexon11 variant, and 3 patients with PIK3CA-Related Overgrowth Spectrum (PROS) caused by the activating *PIK3CA* mutations indicated. (A) Immunoblots, with the truncated p85α Δexon11 variant arrowed; (B)-(E) quantification of immunoblot bands from 3 independent experiments shown for phosphoAKT-S473, phosphoAKT-T308, p110δ and p110α respectively. Paired datapoints +/- insulin are shown in (B) and (C), and dotted lines mark means. Asterisks indicate a significant difference. More detailed statistical analysis including 95% confidence intervals for the paired mean differences for these comparisons are shown in Figure EV2.

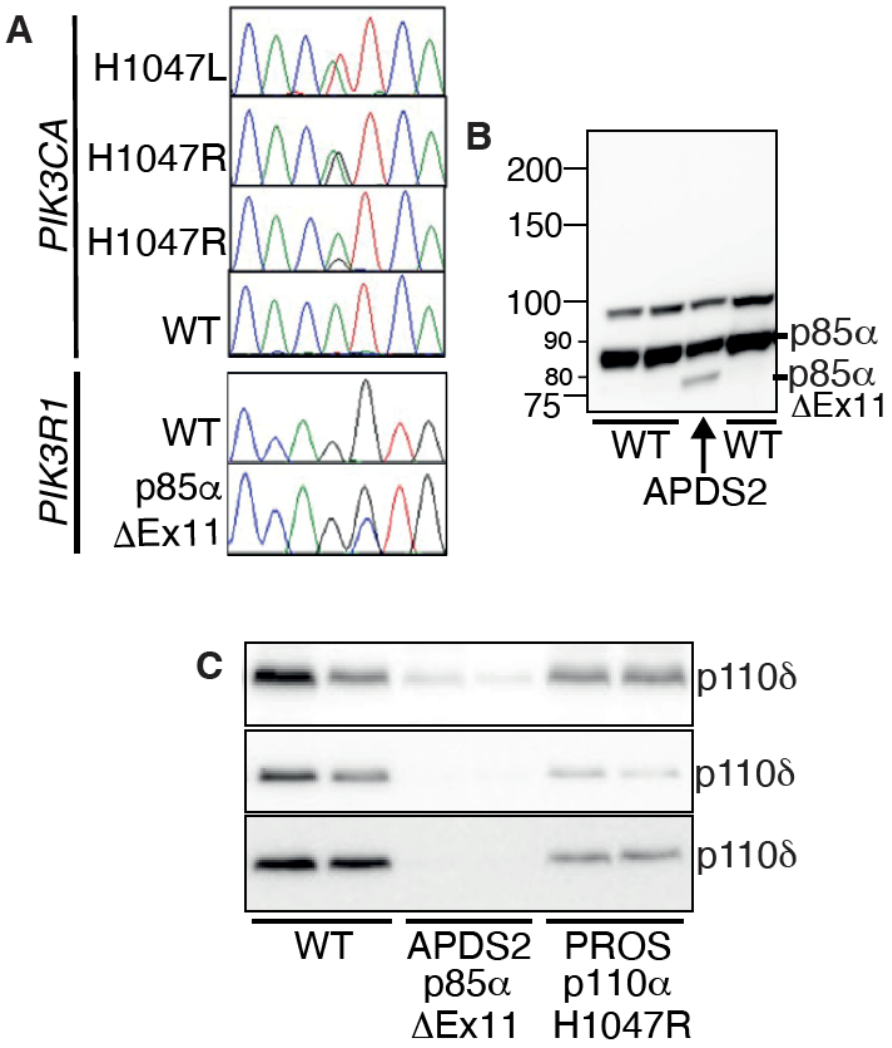

Figure 1 supplement 1. Further characterisation of primary dermal fibroblasts studied. (A) Details of cDNA sequence for *PIK3CA* and *PIK3R1* from cells derived from healthy controls (WT), patients with APDS2 (p85α ΔEx11) or *PIK3CA*-related overgrowth syndrome (PROS), confirming expected expression of mutant alleles. (B) Higher magnification detail of immunoblot from wild-type and APDS2 fibroblasts showing truncated p85α Δex11. (C) All 3 immunoblot replicates for p110δ blots quantified in Figure 1, showing severely reduced p110δ expression in the APDS2 cell line

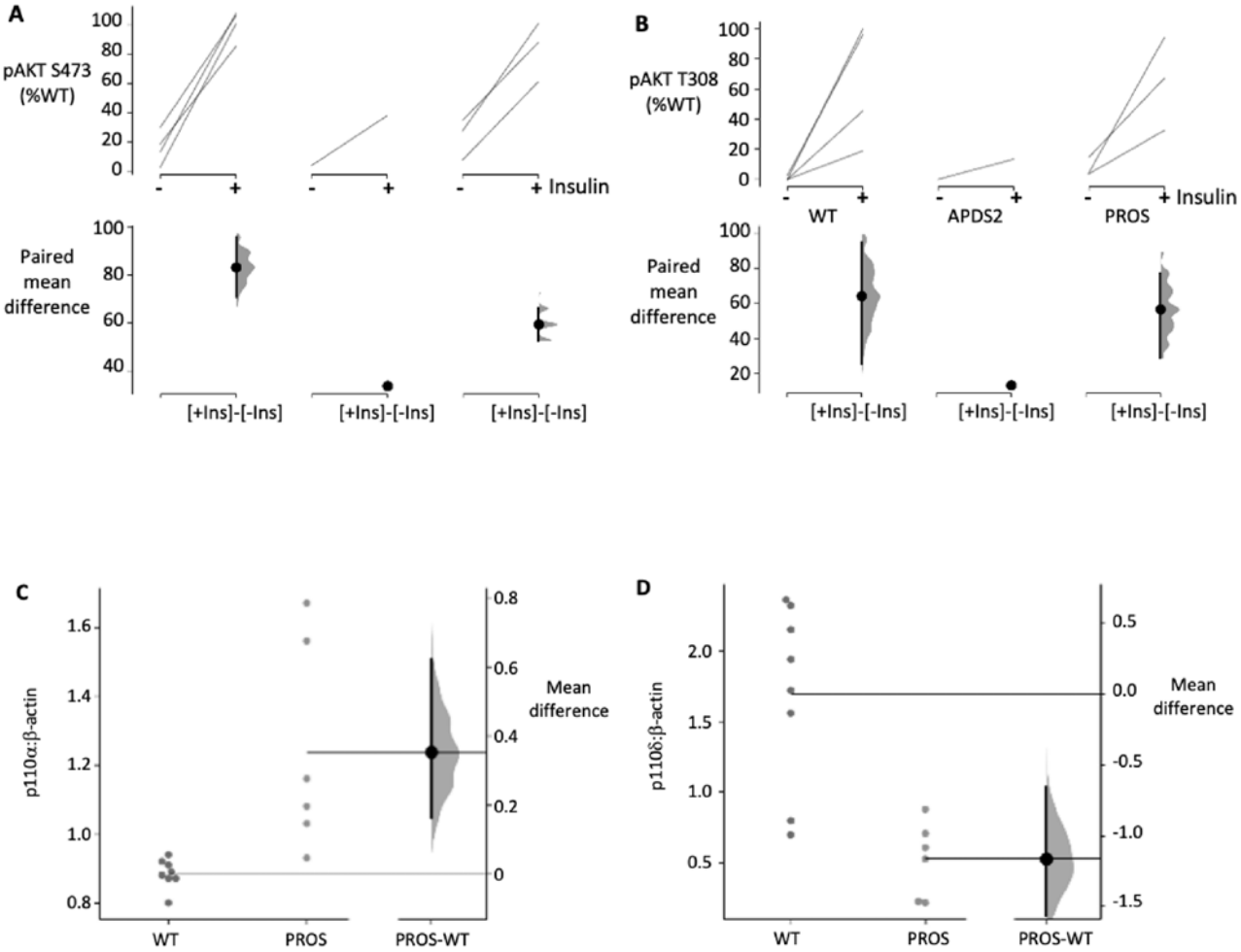

Figure 1 supplement 2. Full statistical analysis of data presented in main Figure 1 Analysis of insulin-induced increase in (A) AKT S473/4 and (B) T308/9 phosphorylation. The paired mean difference for 3-4 comparisons are shown in Cumming estimation plots. The raw data, as presented in Figure 1, are re-plotted on the upper axes with paired observations connected by a line. On the lower axes, paired mean differences are plotted as a bootstrap sampling distribution. Mean differences are depicted as dots; 95% confidence intervals are indicated by the ends of the vertical error bars. (C-D) Analysis of differences in (C) p110α and (D) p110δ protein expression between healthy control cells and cells from PROS patients harbouring activating PIK3CA mutations. Mean differences are shown in Gardner-Altman estimation plots, with expression data plotted on the left axes and mean difference on floating axes on the right, again as a bootstrap sampling distribution with mean difference depicted as a dot and 95% confidence intervals by the ends of the vertical bar.

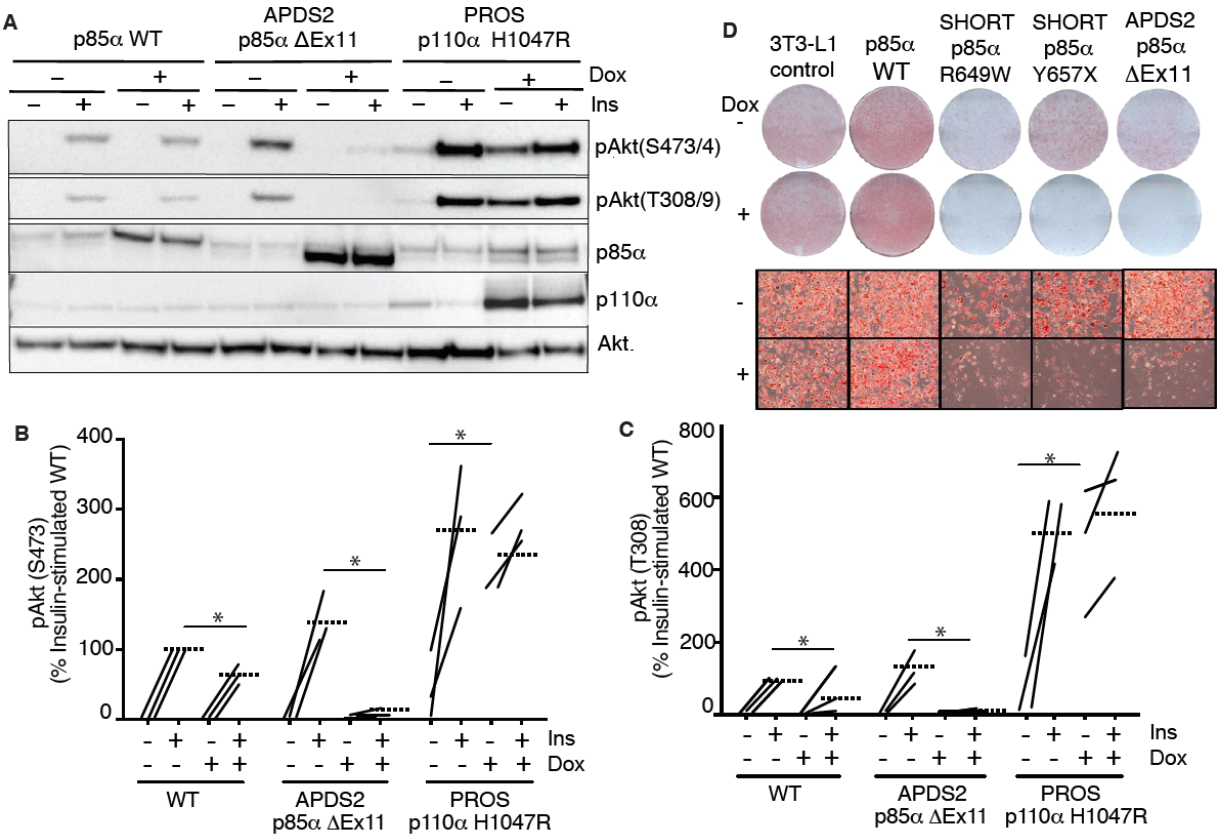

Figure 2. Blunted insulin signaling in 3T3-L1 preadipocyte models of APDS2 and SHORT syndrome. Immunoblotting of Akt, Akt phosphorylated at threonine 308 (T308) or serine 473 (S473), p85α, and p110α and are shown with and without stimulation with 100 nM insulin (Ins) for 10 minutes. Cells were treated with doxycycline (Dox) 1μg/mL for 72 hours prior to insulin stimulation as indicated. (A) One immunoblot representing 3 experiments is shown. (B)-(C) Quantification of immunoblot bands from all 3 independent experiments shown for phosphoAkt-S473 and phosphoAkt-T308 respectively. Paired datapoints +/- insulin are shown, and dotted lines mark means. Asterisks indicate a significant difference. More detailed statistical analysis including 95% confidence intervals for the paired mean differences for these comparisons are shown in Figure EV3. (D) Staining for neutral lipid with Oil Red O of 3T3-L1 cells at day 10 of adipocyte differentiation. Induction of transgene expression by 1μg/mL doxycycline throughout differentiation is shown. Images of entire plates are shown above, with representative bright field microscopy images below.

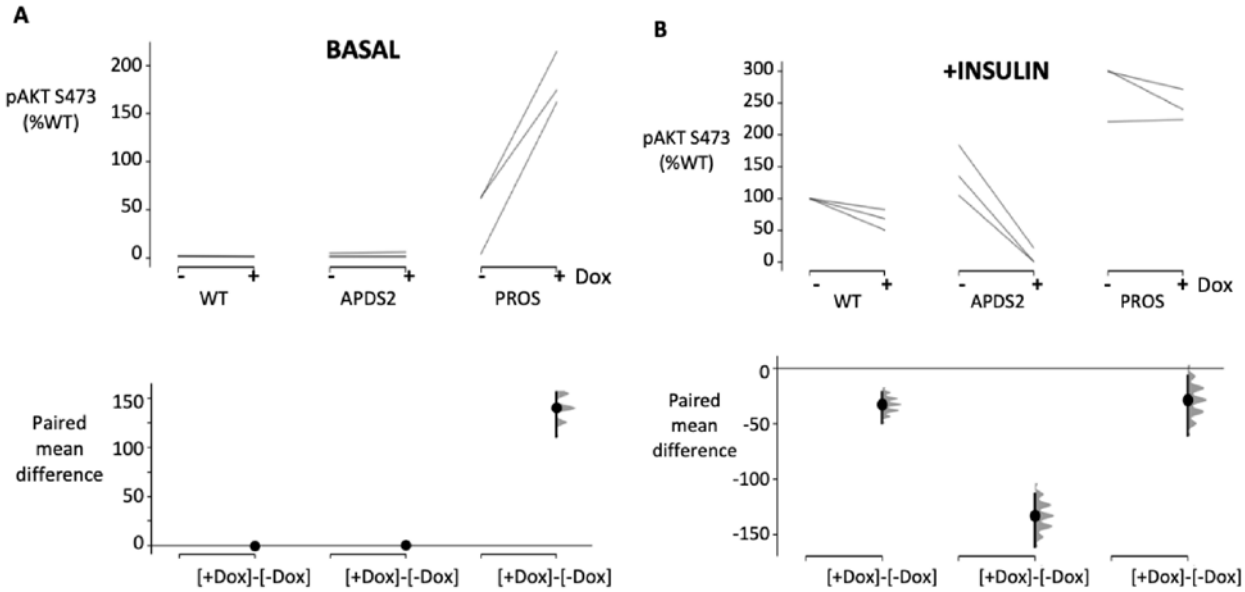

Figure 2 supplement 1. Full statistical analysis of data presented in main Figure 2. Analysis of the effects of doxycycline-induced expression of wild-type (WT) or ΔEx11 (APDS2) p85α, or of p110α H1047R (PROS) on Akt S473/4 (A,B) and T308/9 (C,D) phosphorylation. Comparisons are made in both the basal, non-insulin stimulated state (A,C) and after stimulation with 10 nmol/L insulin (B,D). Paired mean differences for 3 comparisons are shown in Cumming estimation plots. Raw data, as presented in Figure 2, are re-plotted on the upper axes with paired observations connected by a line. On the lower axes, paired mean differences are plotted as a bootstrap sampling distribution. Mean differences are depicted as dots; 95% confidence intervals are indicated by the ends of the vertical error bars.

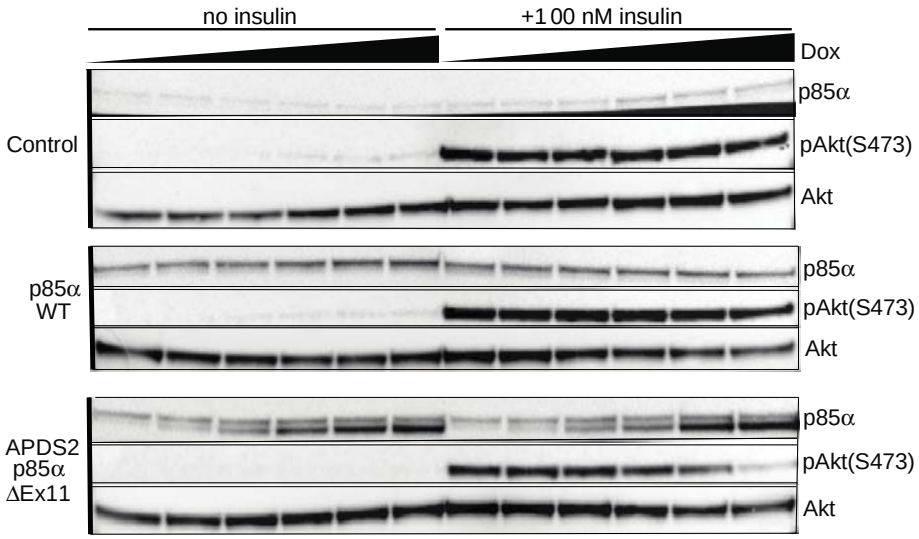

Figure 2 supplement 2. The effect of graded expression of wild-type or disease-associated p85α on 3T3-L1 preadipocytes. Immunoblots of p85α, phosphoAkt (S473) and total Akt are shown for control 3T3-L1 cells and 3T3-L1 cells conditionally expressing wild-type (WT), or APDS2-associated mutant p85α under the control of doxycycline (Dox), with and without 10 minutes of exposure to insulin as indicated. The filled black triangles indicate increasing concentrations of doxycycline (from left to right: 0, 0.02, 0.03, 0.045, 0.065, or 0.1 μg/mL). Exposure was for 72 hours in all cases. The truncated p85α variant can be seen below the WT p85α for the APDS2 ΔEx11 mutant.

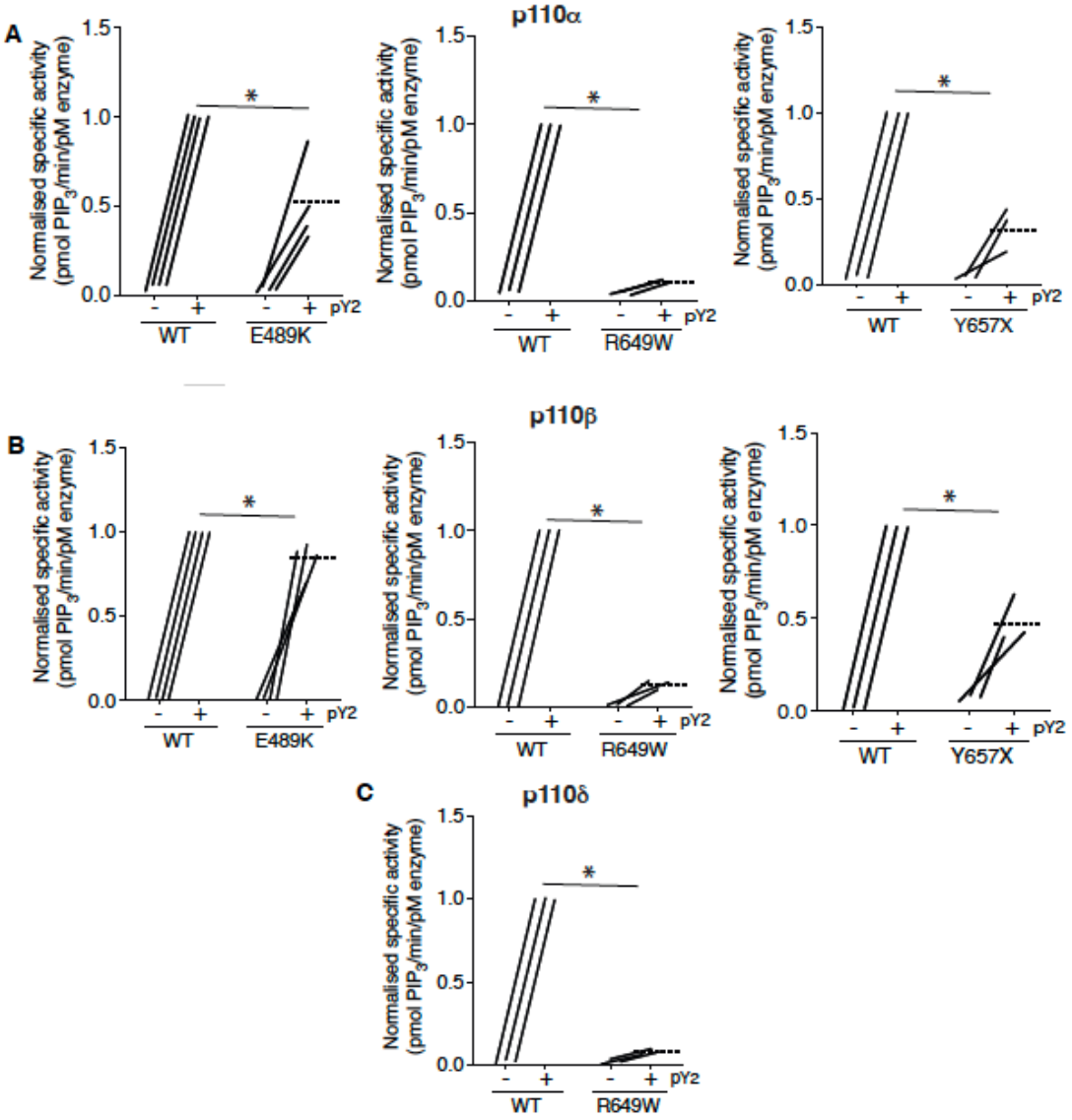

Figure 3. SHORT syndrome p85α mutations impair phosphotyrosine-stimulated phosphoinositide 3-kinase activity. Lipid kinase activity of purified recombinant PI3K complexes generated using baculoviral expression in *Sf9* cells was measured using a modified fluorescence polarisation assay. WT p85α or p85α SHORT syndrome mutations, E489K, R649W or Y657X bound to either (A) p110α (B) p110β or (C) p110δ were assayed for basal and bisphosphotyrosine (pY2)-stimulated lipid kinase activity. Dotted lines mark means, and asterisks indicate a significant difference between the bisphosphotyrosine (pY2)-stimulated state for WT and comparator mutant p85α. More detailed statistical analysis including 95% confidence intervals for the paired mean differences for these comparisons are shown in Figure EV5.

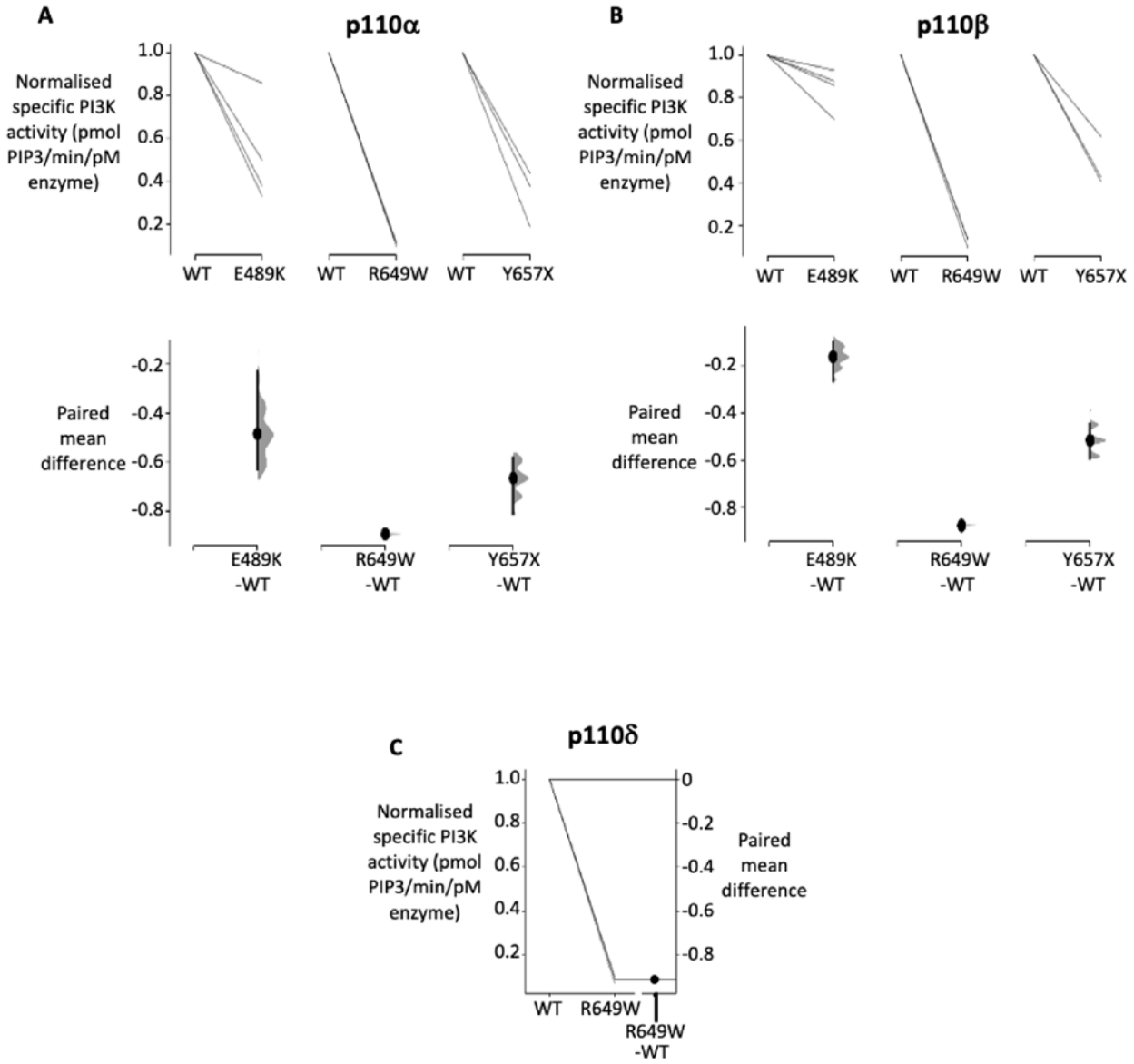

Figure 3 supplement 1. Full statistical analysis of data presented in main Figure 3. Analysis of fluorescence polarisation assay of phosphoinositide 3-kinase (PI3K) activity of *in vitro* synthesised wild-type (WT) or mutant (E489K, R649W or Y657X) p85α. Results for p110α- and p110β-containing PI3K are shown in (A) and (B) respectively. All data were acquired in the presence of phosphotyrosine peptide. Paired mean differences for 3 comparisons are shown in Cumming estimation plots. Raw data, as presented in Figure 3, are re-plotted on the upper axes with paired observations connected by a line. On the lower axes, paired mean differences are plotted as a bootstrap sampling distribution. Mean differences are depicted as dots; 95% confidence intervals are indicated by the ends of the vertical error bars. Results for the R649W p85α mutation only are shown with p110δ in (C).

In this case raw data are re-plotted on the left hand axes with paired observations connected by 3 nearly superimposed lines. On the right hand axes, paired mean differences are plotted as a bootstrap sampling distribution.

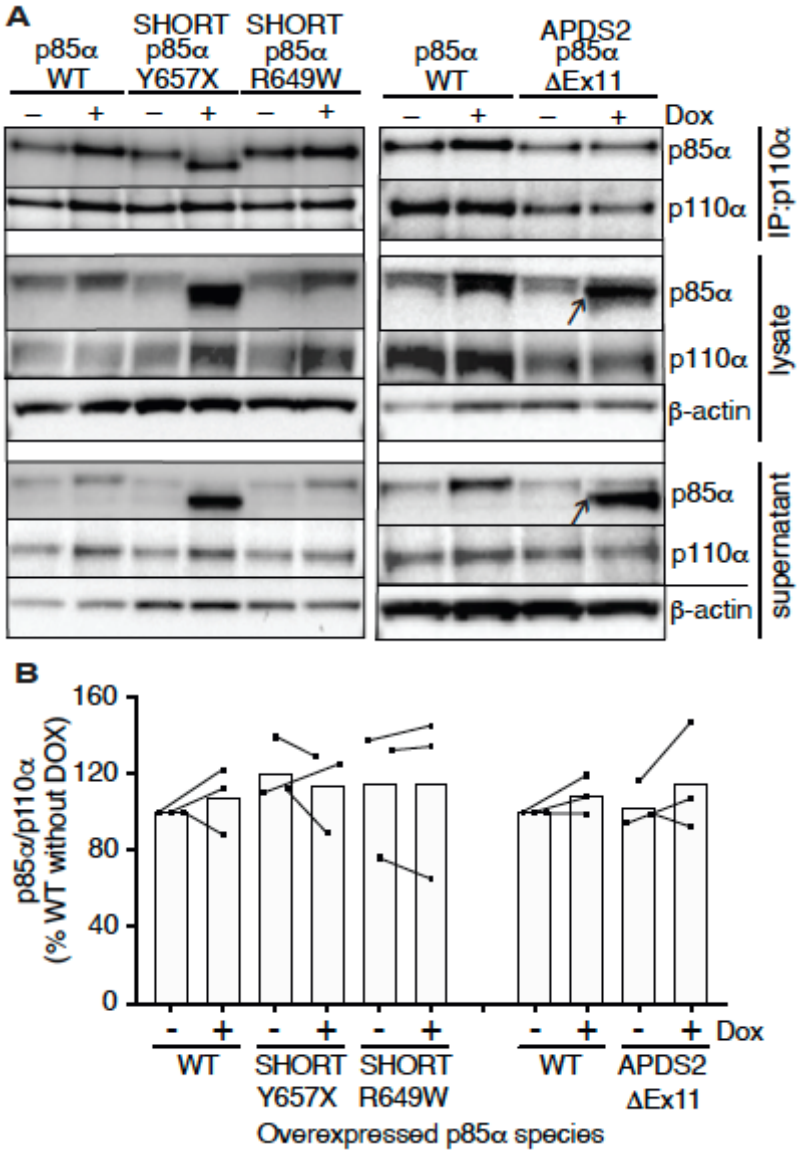

Figure 4. Ability of pathogenic p85α variants to bind p110α, assessed by co-immunoprecipitation. Results of immunoblotting of anti-p110α immunoprecipitates from 3T3-L1 cells expressing wild-type, APDS2-associated or SHORT syndrome-associated mutant p85α under the control of doxycycline (Dox) are shown. (A) One representative immunoblot of immunoprecipitate, cell lysate prior to immunoprecipitation, and post immunoprecipitation supernatant is shown. (B) Quantification of immunoblot bands from immunoprecipitates from 3 independent experiments. Co-immunoprecipitated p85α is shown normalized to immunoprecipitated p110α from all 3 independent experiments. Datapoints from the same experiment +/- doxycline are connected by lines. No significant differences were found among conditions.

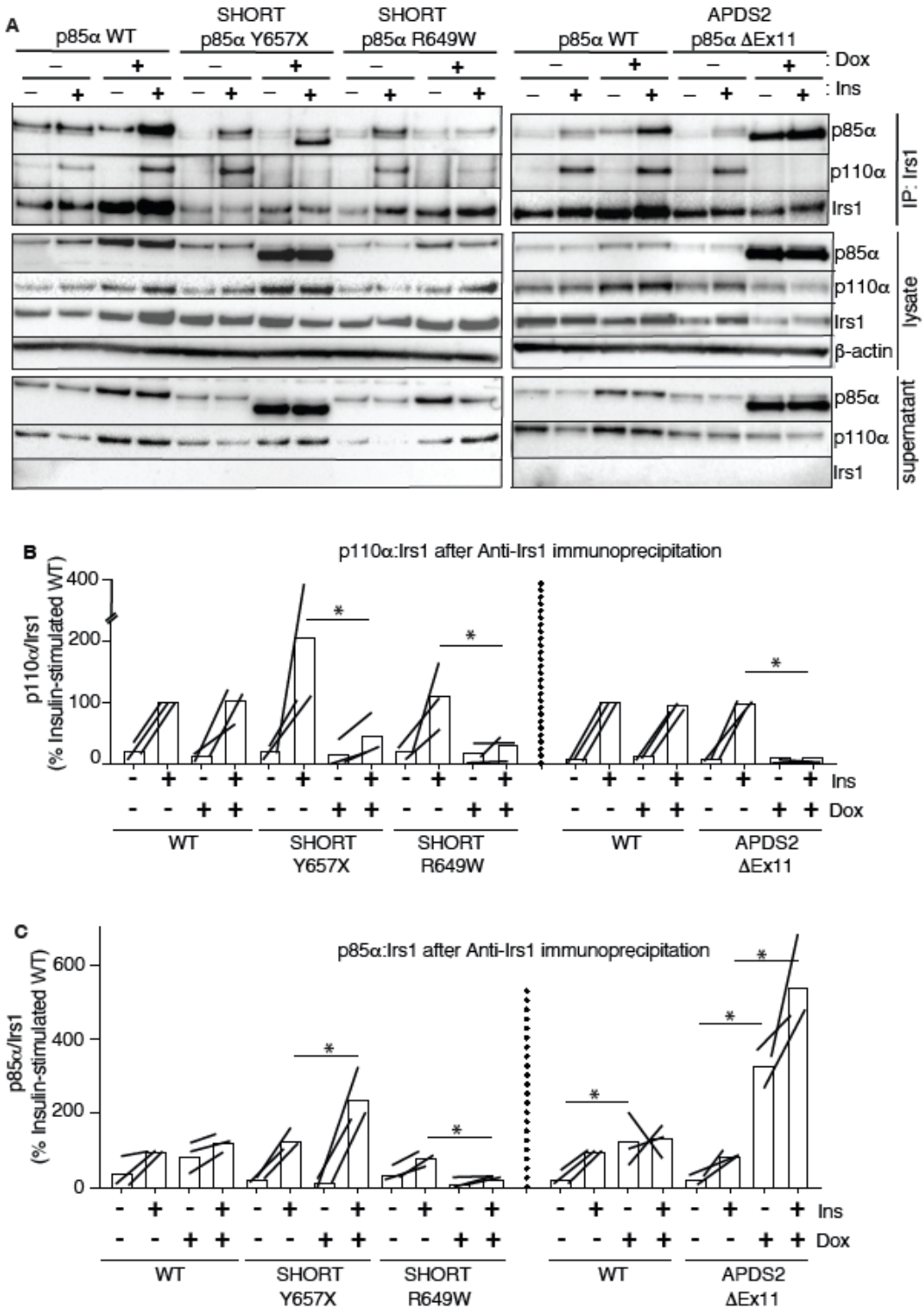

Figure 5. Attenuated insulin-induced association of p110α with Irs1 in the presence of APDS2 and SHORT syndrome mutant p85α. Results of immunoblotting of anti-Irs1 immunoprecipitates from 3T3-L1 cells expressing wild-type, APDS2-associated or SHORT syndrome-associated mutant p85α under the control of doxycycline (Dox) are shown.

Treatment with 100nM insulin (Ins) is indicated. (A) One representative immunoblot of immunoprecipitate, cell lysate prior to immunoprecipitation, and post immunoprecipitation supernatant is shown. Two separate sets of gels, including independent wild-type controls are shown on left and right. (B-C) Quantification of immunoblot bands from immunoprecipitates from 3 independent experiments. Immunoprecipitated p110α is shown normalized to immunoprecipitated Irs1 from all 3 independent experiments in (B), and immunoprecipitated p85α similarly in (C). Datapoints from the same experiment +/- insulin are connected by lines. Asterisks indicate significant differences induced by transgene overexpression (i.e. plus versus minus doxycycline). More detailed statistical analysis including 95% confidence intervals for the paired mean differences for these comparisons are shown in Figure EV6.

890

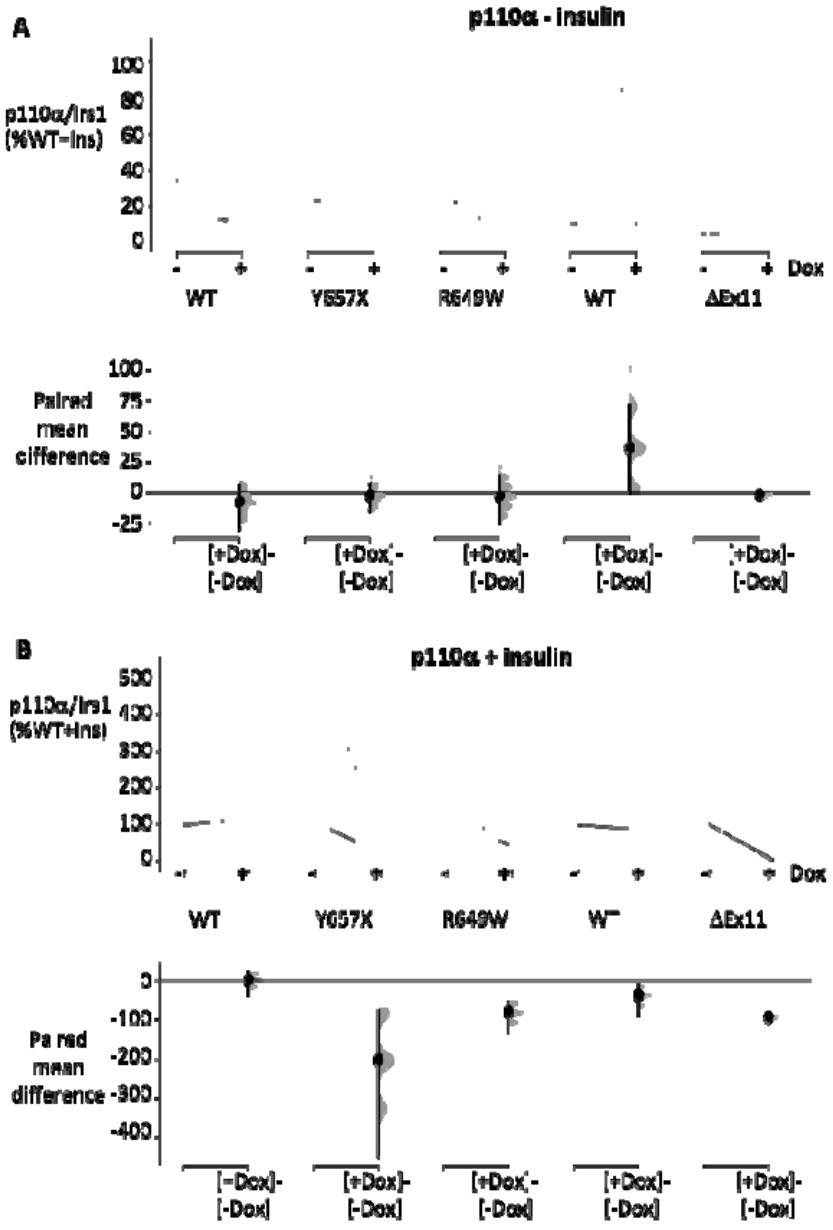
A
p110α - insulin
p110α/Irs1
(%WT-Ins)
100
80
60
40
20
0
Dox
WT
Y657X
R649W
WT
ΔEx11
Paired
mean
difference
100
75
50
25
0
-25
[+Dox]-
[-Dox]
B
p110α + insulin
p110α/Irs1
(%WT+Ins)
500
400
300
200
100
0
Dox
WT
Y657X
R649W
WT
ΔEx11
Paired
mean
difference
0
-100
-200
-300
-400
[-Dox]-
[-Dox]
[+Dox]-
[-Dox]

891

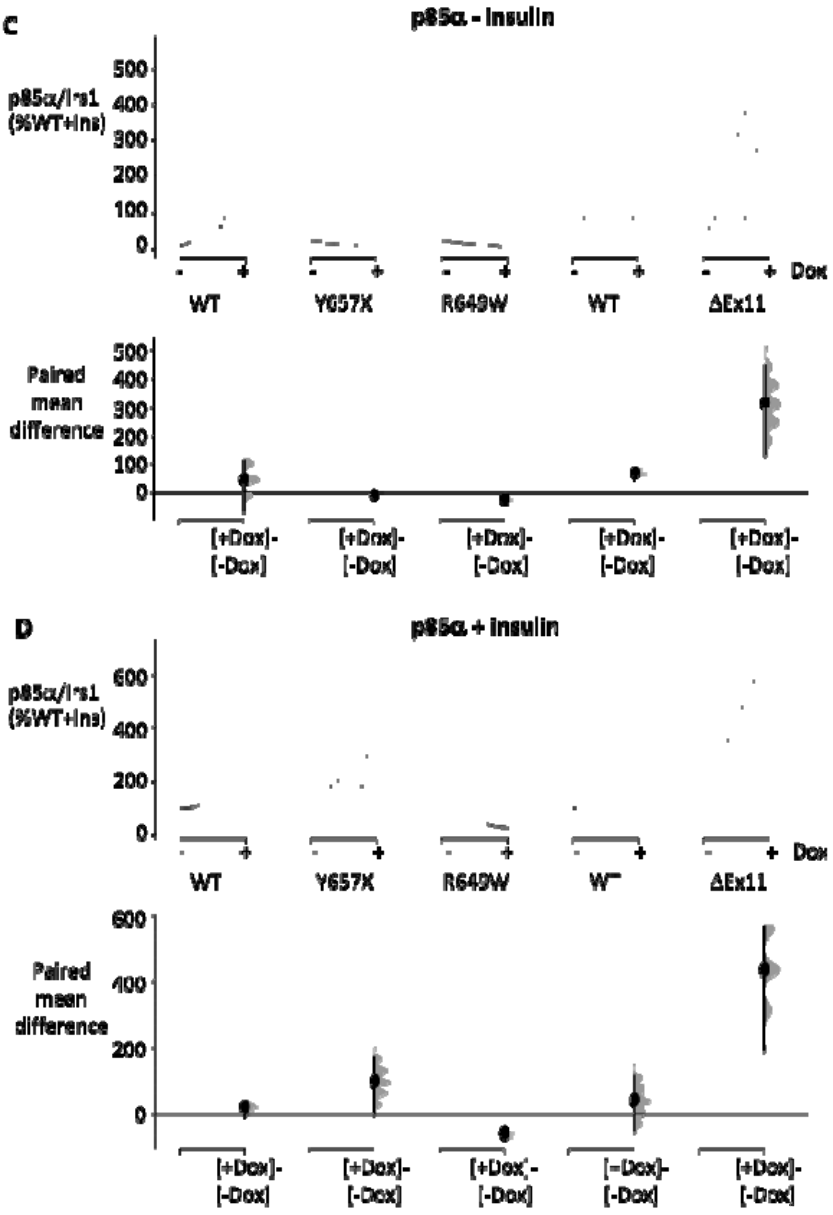

892

893 **Figure EV5 supplement 1. Full statistical analysis of data presented in main Figure 5.**
894 Analysis of the effects of doxycycline (dox)-induced expression of wild-type (WT), Y657X,
895 R649W or ΔEx11 p85α on association of p110α (A,B) and p85α (C,D) with Irs1. Results of
896 co-immunoprecipitation with (B,D) and without exposure to 10 nmol/L insulin Comparisons
897 are made in both the basal, non-insulin stimulated state (A,C) and after stimulation with 10
898 nmol/L insulin (B,D) are shown. Paired mean differences for 3 comparisons are shown in
899 Cumming estimation plots. Raw data, as presented in Figure 5, are re-plotted on the upper
900 axes with paired observations connected by a line. On the lower axes, paired mean
901 differences are plotted as a bootstrap sampling distribution. Mean differences are depicted
902 as dots; 95% confidence intervals are indicated by the ends of the vertical error bars.

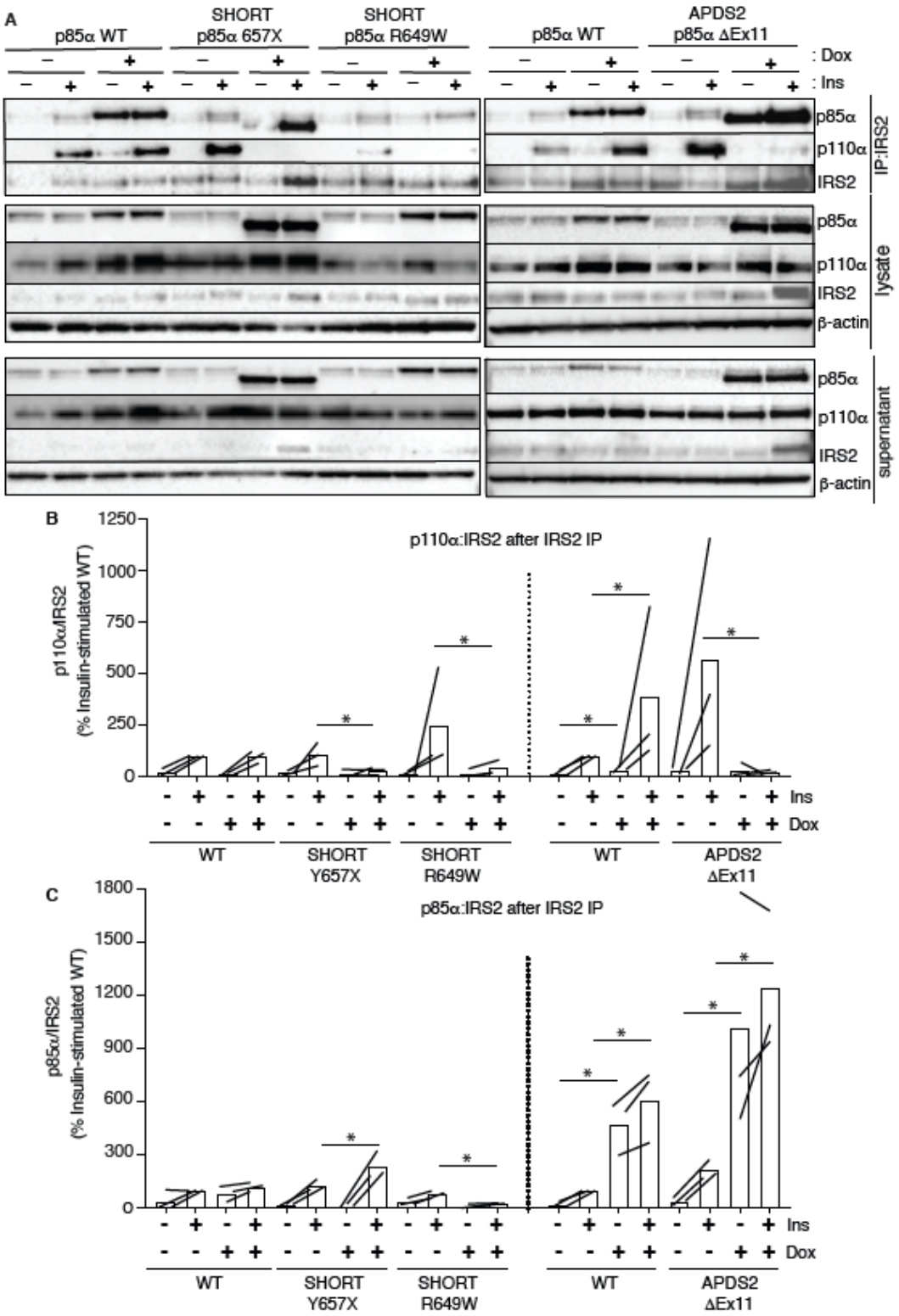

Figure 6. Attenuated insulin-induced association of p110α with Irs2 in the presence of APDS2 and SHORT syndrome mutant p85α. Results of immunoblotting of anti-Irs2 immunoprecipitates from 3T3-L1 cells expressing wild-type, APDS2-associated or SHORT syndrome-associated mutant p85α under the control of doxycycline (Dox) are shown.

Treatment with 100nM insulin (Ins) is indicated. (A) One representative immunoblot of immunoprecipitate, cell lysate prior to immunoprecipitation, and post immunoprecipitation supernatant is shown. Two separate sets of gels, including independent wild-type controls are shown on left and right. (B-C) Quantification of immunoblot bands from immunoprecipitates from 3 independent experiments. Immunoprecipitated p110α is shown normalized to immunoprecipitated Irs2 from all 3 independent experiments in (B), and immunoprecipitated p85α similarly in (C). Datapoints from the same experiment +/- insulin are connected by lines.

917

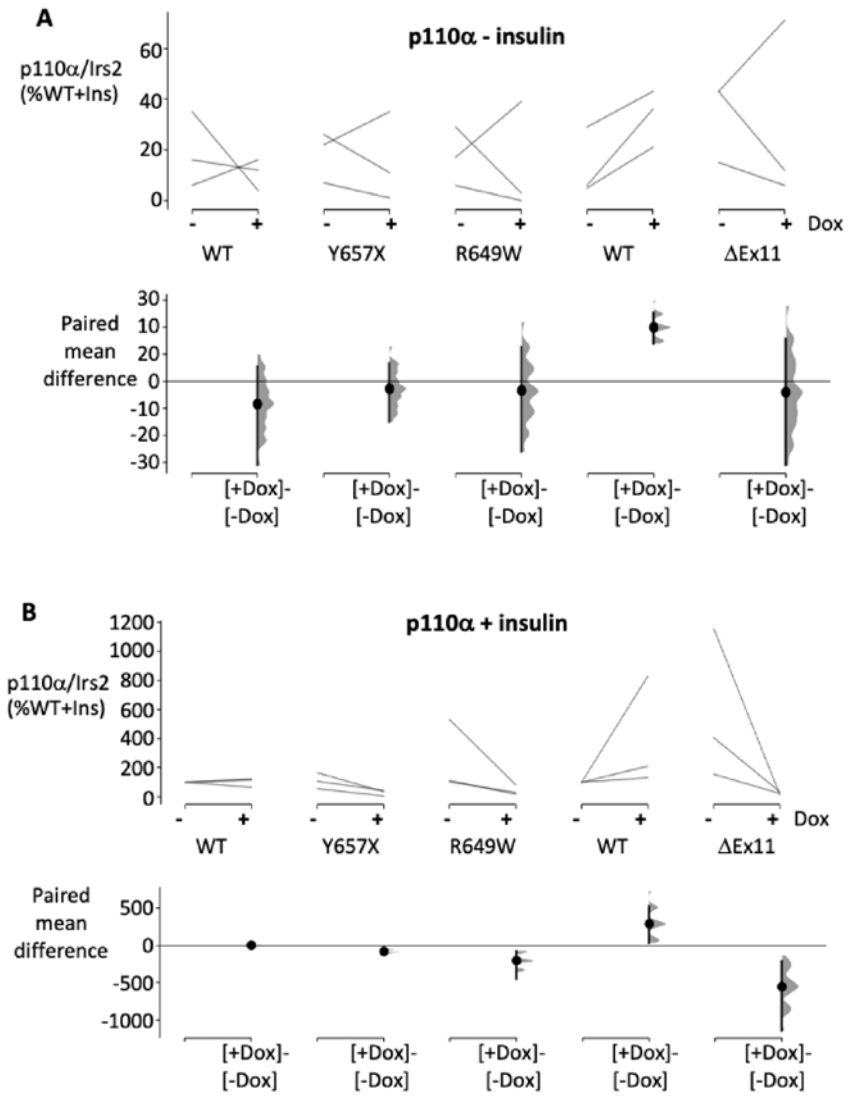
A
p110α - insulin
p110α/Irs2
(%WT+Ins)
60
40
20
0
- +
Dox
WT
Y657X
R649W
WT
ΔEx11
Paired
mean
difference
30
10
20
0
-10
-20
-30
[+Dox]-
[-Dox]
B
p110α + insulin
p110α/Irs2
(%WT+Ins)
1200
1000
800
600
400
200
0
Paired
mean
difference
500
0
-500
-1000

918

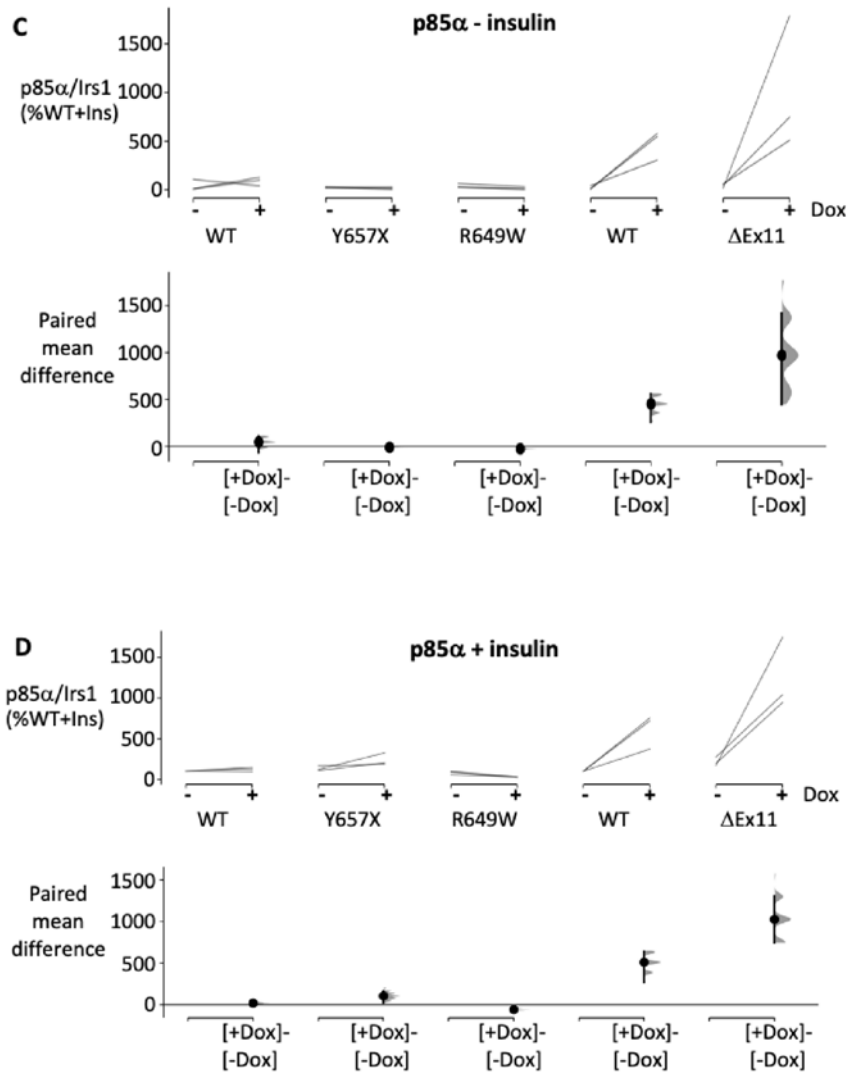

Figure 6 supplement 1. Full statistical analysis of data presented in Figure EV7. Analysis of the effects of doxycycline (dox)-induced expression of wild-type (WT), Y657X, R649W or ΔEx11 p85α on association of p110α (A,B) and p85α (C,D) with Irs2. Results of co-immunoprecipitation with (B,D) and without exposure to 10 nmol/L insulin Comparisons are made in both the basal, non-insulin stimulated state (A,C) and after stimulation with 10 nmol/L insulin (B,D). Paired mean differences for 3 comparisons are shown in Cumming estimation plots. Raw data, as presented in Figure EV7, are re-plotted on the upper axes with paired observations connected by a line. On the lower axes, paired mean differences are plotted as a bootstrap sampling distribution. Mean differences are depicted as dots; 95% confidence intervals are indicated by the ends of the vertical error bars.

Table

Antibody	Company	Catalogue No.	Species	Dilution used (immunoblot/IP)
p85α	CST	4257	Rabbit	1:1000
Phospho-AKT/Akt (T308)	CST	9275	Rabbit	1:1000
Phospho-AKT/Akt (S473)	CST	9271	Rabbit	1:1000
AKT/Akt (1,2,3)	CST	2920	Mouse	1:1000
p110α	CST	4249	Rabbit	1:1000/1:50
p110δ	CST	34050	Rabbit	1:1000
Irs1	Millipore	06-248	Rabbit	1:500
Irs1	CST	2382	Rabbit	1:1000/1:50
Irs2 clone 9.52	Millipore	MABS15	Mouse	1:1000/1:50
β-actin	CST	4967	Rabbit	1:5000
Anti-rabbit IgG; HRP-linked	CST	7074	Goat	1:5000
Anti-mouse IgG; HRP-linked	CST	7076	Horse	1:5000

Table 1: Antibodies Used